ROBUST CONTROL OF GEARED AND DIRECT-DRIVE ROBOTIC MANIPULATORS UNDER PARAMETER AND MODEL UNCERTAINTIES

By

Praveen Reddy Suravaram

RECOMMENDED:

John Aspnes

Dr. John Aspnes

C.S. Sonwalkar

Dr. Vikas Sonwalkar

Dr. Seta Bogosyan, Advisory Committee Chair

C.S. Sonwalkar

Chair, Department of Electrical and Computer Engineering

APPROVED:

John Aspnes

Dean, College of Engineering and Mines

Susan A. Henrichs

Dean of the Graduate School

April 26, 2005

Date

ROBUST CONTROL OF GEARED AND DIRECT-DRIVE ROBOTIC MANIPULATORS UNDER PARAMETER AND MODEL UNCERTAINTIES

A

THESIS

Presented to the Faculty

of the University of Alaska Fairbanks

in Partial Fulfillment of the Requirements

for the Degree of

MASTER OF SCIENCE

By

Praveen Reddy Suravaram, B. Tech

Fairbanks, Alaska

May 2005

ABSTRACT

The major contribution of this thesis is the design and evaluation of a chattering-free sliding mode controller (SMC), which is a novel application for 2 degree-of-freedom (DOF) planar robot arms exposed to load variations. The performance of the SMC is evaluated in comparison to a proportional-derivative-plus (PD+) controller, as an example of nonlinear model-based controllers, as well as classical linear controllers, such as proportional-derivative (PD) and proportional-integral-derivative (PID). The performance of all four methods has been tested via realistic and detailed simulation models developed for both geared and direct-drive type 2-DOF planar robot arms. The model used in simulations reflects the dynamics of the arm, as well as the actuator dynamics and pulse width modulation (PWM) switching of the power converters. Simulations are performed under unknown load variations for both step and sinusoidal type reference joint trajectories. The results demonstrate that the chattering-free SMC provides increased accuracy and robustness than that of the other controllers and requires no prior knowledge of the system dynamic model and the load variation that the end-effector is subjected to. The results obtained could be extended to the control of a variety of geared and direct-drive type robotic configurations.

Table of Contents

List of Figures

List of Tables

Acknowledgements

It gives me great pleasure to thank all the individuals that supported me in this work. I would like to gratefully acknowledge the guidance and encouragement received from my advisor Dr. Seta Bogosyan. I express my sincere thanks for her time and patience. I pay my sincere thanks to Dr. Metin Gokasan for helping me through out my thesis. I want to acknowledge my committee members Dr. John Aspnes and Dr. Vikas Sonwalkar for their suggestions and valuable comments.

I want to thank my family members and friends for standing with me, providing moral support and encouraging me throughout my career.

1. INTRODUCTION

1.1 Thesis Objective

The main objective of this thesis is to provide a basis of evaluation for the most widely used robot control approaches, with regards to parameter and model uncertainties as well as external disturbances caused by the load variation. As an example of robotic configurations exposed to load uncertainties, a two degree of freedom (DOF) planar robotic arm is considered. Four controllers are developed for the position and trajectory control of the arm; namely, PD and PID controllers as standard linear controllers, PD+ as a nonlinear model based controller, and finally, a chattering-free sliding mode controller (SMC), as an example of a robust controller. The developed SMC is a novel application for the control of robot arms under load uncertainties and requires minimum a priori knowledge of the system model. All four methods are evaluated by simulations for step-type and sinusoidal trajectories applied directly as joint references. Additionally, the controllers are tested for both the geared and direct-drive configurations of a 2-DOF robot arm.

1.2 Robot Manipulators

According to the Robot Institute of America, a robot is defined as a reprogrammable multifunctional manipulator designed to move material, parts, tools, or specialized devices through variable programmed motions for the performance of a variety of tasks. Robot manipulators are an important class of robots and are primarily used in materials handling, assembly, spray painting, welding, deburring, grinding, and other manufacturing applications.

Robot manipulators are basically composed of rigid links connected by joints into a kinematic chain, which allows the relative motion of neighboring links. The joints of manipulator arms can be of four types:

- Revolute or pin joint

- Prismatic or sliding joint
- Screw joint
- Spherical joint

Revolute joints allow relative rotation between two neighboring links and the displacements caused by them are called joint angles. A prismatic or sliding joint allows linear relative motion or translation, which is sometimes called "joint offset". The screw joint allows a helical motion between the two links. A bolt and nut is a good example for this kind of a joint. The spherical joint allows one link to rotate in all possible directions with respect to the second link. At the final end of all links of a manipulator is the end-effector, which could be any device (usually a gripper or tool) depending on the application.

An important term associated with any mechanical system is degrees of freedom (DOF). The number of independent variables required to specify the motion of the system represents the degrees of freedom of the manipulator. In order to reach and grab a material or object in free space, a manipulator should possess at least six degrees of freedom: 3-DOFs for positioning (x, y, z) and 3-DOF for orientation around the three axes (x, y, z). As an example of a six degree of freedom robot manipulator, the PUMA 560 manipulator is shown in Fig.1.1. The PUMA 560 is a popular robot manipulator used in industries.

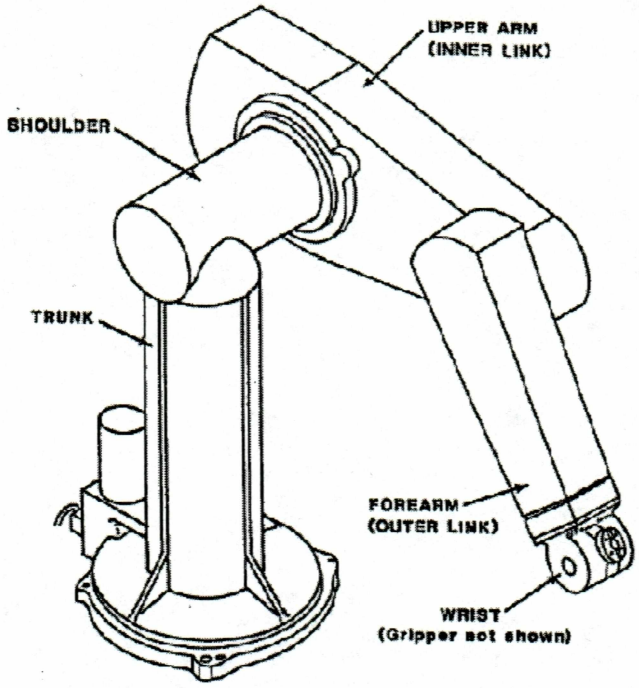

Fig. 1.1 A six degrees of freedom PUMA 560 manipulator.
(Source:http://www.seas.upenn.edu)

1.3 Kinematics of Manipulators

Kinematics involves the study of position, velocity, acceleration and all higher order derivatives of position variables of the manipulator with respect to time or any other variables. Kinematics can be categorized in 3 groups: forward, inverse and velocity kinematics.

Forward kinematics: It determines the position and the orientation of the end-effector of the manipulator for a given set of joint variables. Forward kinematics can be represented mathematically as below:

$$X = f(\theta) \tag{1.1}$$

where,

$$\theta = \begin{bmatrix} \theta_1 \\ \theta_2 \\ \vdots \\ \vdots \\ \theta_n \end{bmatrix}$$

In the above equation, X represents the position and orientation of the end-effector and θ is the set of joint variables of the manipulator. Any manipulator arm consists of a series of links connected by 1-DOF rotational or prismatic joints. There is a virtual frame attached to each link, which is used to describe the position and orientation of that system. Many methods are available to describe the mechanisms, but the most popular and widely used approach is the Denavit-Hartenberg (D-H) representation. A 4 × 4 homogeneous transformation matrix is formed using D-H representation, which gives the description of a link's position and orientation with respect to the previous link. Using this approach, any link frame can be expressed with respect to the base coordinate frame or any other frame of choice.

Inverse kinematics: It deals with the calculation of joint variables for a given position and orientation of the end-effector. The mathematical representation of inverse kinematics can be given as follows:

$$\theta = f^{-1}(X) \tag{1.2}$$

where X is the position and orientation of the end-effector and θ is the set of joint variables of the manipulator.

The inverse kinematics problem can be solved by either taking an algebraic or geometric approach. A unique solution may not be obtained, as the joint coordinates for a given end-effector position and orientation are not unique (in general). An example of

multiple solutions for a given end-effector position and orientation is illustrated in Fig.1.2 for a three-link manipulator.

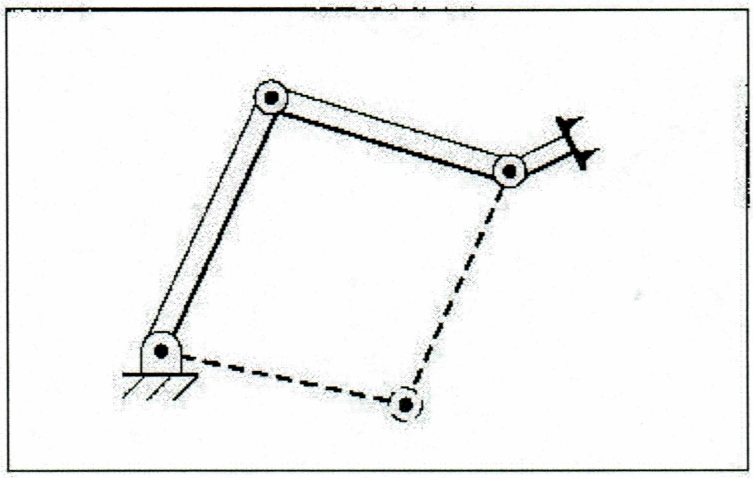

Fig. 1.2 A 3DOF manipulator with two possible solutions.
(Source: Craig, 1989)

If the manipulator has two solutions, it has to be able to choose one and the reasonable solution is the closest solution which minimizes the amount that each joint should move. The selection of solutions may change if the manipulator has an obstacle in the closer solution or an unexpected load variation has occurred. In this case, it may have to switch to the other solutions for a given end-effector position and orientation. The number of solutions increases with increasing number of joints involved in a manipulator and as a result, the inverse kinematic solutions become more complex. In the literature, it is possible to find the inverse kinematic solutions for common manipulator configurations, but with every novel configuration, new and efficient methods must be sought for inverse kinematics [Craig, 1989].

Velocity kinematics: It deals with the analysis of velocity relationships relating the linear and angular velocities of the end-effector to the linear and angular velocities of the joints of the manipulator. The velocity relationships are expressed in the vector form by a

matrix called the Jacobian or Jacobian Matrix. The Jacobian is a multidimensional form of the derivative. For example, we have a set of functions, each of which is a function of some independent variables, which can be represented in vector notation as

$$Y_n = F(X_n) \tag{1.3}$$

Now, in order to calculate the differential of Y_n as a function of differentials of X_n,

$$\delta Y_n = \frac{\partial F}{\partial X_n} \delta X_n \tag{1.4}$$

The n × n matrix of partial derivatives in the above equation is called the Jacobian. By dividing the differential time element, we get the Jacobian as a mapping of velocities in X to those in Y:

$$\dot{Y}_n = J(X_n)\dot{X}_n \tag{1.5a}$$

In the case of robotics, (1.5a) gives rise to the relation between joint velocities and end-effector velocity, such as,

$$V = J(\theta)\dot{\theta} \tag{1.5b}$$

The Jacobian plays an important role in the analysis and control of motion to get smooth trajectories and in the derivation of dynamic equations of manipulator arms.

1.4 Dynamics of Manipulators

Robot dynamics deals with the calculation of forces/torques, which are required to cause motion. Robot manipulators are basically positioning devices. In order to move or place an object by the end-effector, the joint actuators of a manipulator should be given a set of torque/force functions. This set of torque/force functions can be obtained by formulating dynamic equations of the manipulator, which can be represented as below in its general form:

$$\tau = M(\Theta)\ddot{\Theta} + C(\Theta, \dot{\Theta}) + G(\Theta) \tag{1.6}$$

where τ is the torque required to cause motion;

$M(\Theta)$ is the n ×n mass or inertia matrix of the manipulator;

$C(\Theta, \dot{\Theta})$ is an n × 1 vector of centrifugal and coriolis terms;

$G(\Theta)$ is an n × 1 vector of gravity terms, (terms that include gravitational acceleration, g).

The dynamic equations of motion may also be used to give information on joint actuator dynamics, friction effects, joint and link flexibility, and external disturbances. Knowledge of the dynamics of robotic manipulators is vital for accurate simulations and for a good control performance, particularly when model-based control schemes are involved.

The dynamic equations of motion can be formulated using two methods: the Newton-Euler method and the Euler-Lagrange method. The first method is a force balance approach and the second is an energy balance approach to dynamics. Both methods will give the same equations of motion for a particular manipulator.

Newton-Euler Formulation: The Newton-Euler equations describe how forces/torques, inertias, and accelerations relate to each other. The derivation involved results in a set of forward and backward recursive equations (dynamic equations). The forward recursion gives kinematic information such as linear velocities, angular velocities, angular accelerations and linear accelerations at the center of mass of each link. The backward recursion propagates the forces and moments exerted on each link from the end-effector to the base reference frame of the manipulator [Spong, 1989]. The dynamic equations derived by this method do not include the dynamics of the control devices, backlash, and gear friction. The significance of this method is that it provides an iterative approach to the solution of dynamic equations and is, therefore, appropriate for computer based applications and the equations could apply to any robot. However, if we wish to have a better insight into the structure of the equations, an analytical approach

might be more appropriate. In that case, the Lagrange-Euler method should be the method of choice for the modeling of the robot dynamics.

Lagrange-Euler Formulation: The Lagrange-Euler formulation offers an analytical method for computing forces/torques. The dynamic equations derived (excluding dynamics of the control devices, and nonlinear effects, such as backlash, and gear friction) are a set of second order coupled nonlinear differential equations. The method utilizes a 4×4 homogenous transformation of the kinematic chain and the Lagrangian formulation; the equations derived are nonlinear and include inertia effects, coriolis and centrifugal forces between joints, and gravity effects. The Lagrange-Euler equations give the closed-form dynamic model of the manipulator, which can be utilized to analyze and design advanced joint variable space control strategies.

1.5 Trajectories

Due to the complexity of kinematics and dynamics of robot manipulators, the motion control problem is generally categorized into three stages: motion planning, trajectory generation, and trajectory tracking. In motion planning, the desired paths are generated in the task space taking obstacles into consideration and without timing information. This means the velocities and accelerations along the paths are not included or specified. In the next stage of the motion control problem, i.e., the trajectory generation, the desired position, velocity, and acceleration along the path are computed as a function of time, either in task space or in joint space [Lewis, 1992]. In this thesis, we assume that motion planning and inverse kinematics are precomputed and proceed with the problem of trajectory tracking, which involves the implementation of a control input to make the joints track a desired trajectory with minimum error in transient and steady-state.

1.6 Control Problem of Robot Manipulators and a Brief Literature Review

The position and tracking control problem of robot manipulators involves development of algorithms to make the end-effector track a desired trajectory with minimum error in spite of structured and unstructured uncertainties and external disturbances. Thus, the problem requires the consideration of a highly nonlinear system under the influence of uncertainties.

In the literature, a variety of control techniques have been developed to address the problem. Linear controllers are mostly based on PD and PID controllers, which is the widely used approach with industrial robots. Even through linear methods provide ease-of-application, for more sophisticated applications and high performance goals, the nonlinear dynamics of the system has to be taken into account when designing control algorithms.

Extensive research has been conducted developing nonlinear control methods for robots. Nonlinear methods can be model-based (i.e. computed torque method, feedback linearization and PD+), for which an accurate model of the system is required. Thus, they are often combined with on-line parameter estimation techniques [Bogosyan and Gokasan, 1995]. There are also robust control techniques based on sliding mode control [Erbatur, 1999]. There are also several studies performing the experimental evaluation of methods, of which some examples can be listed as below: In studies taking the dynamics model of the system into consideration, such as [Kokkinis and Stoughton, 1991], it has been demonstrated through experiments that model-based methods achieved two to four times better performance than the PID control. In [Lu, 1993], control algorithms including PD control, computed torque control and PD plus feedforward have been implemented and model based control methods have been demonstrated to perform best when compared to independent joint controllers. Chen [1993] presented results demonstrating that the computed torque method is more robust than PD plus feedforward control. Kim and Hori [1995] addressed the tracking control of a 2 DOF direct-drive robot arm, for which adaptive and robust control methods were developed. Reyes and

Kelley [2001] performed the experimental comparison of PD and PD+ controllers for a direct drive robot. Comparative studies among robust control schemes have also been reported by [Jaritz and Spong, 1996] and [Liu and Goldenberg, 1996].

1.7 Thesis Outline

The major contribution of this thesis is the design and application of a chattering-free sliding mode controller (SMC), which is a novel application for both geared and direct-drive type robot arms under parameter and model uncertainties and load variations. Besides providing robustness to uncertainties, the aim of the chattering-free SMC is to improve accuracy and not to excite unmodeled dynamics of the system. Simulation results are obtained on a geared type and direct-drive 2-DOF robotic arm, for a PD controller, PID controller, PD+ controller and finally, for the developed SMC while the system is exposed to load variations. Superior results are obtained with the chattering-free SMC which is designed based on the satisfaction of the matching condition and with no a priori consideration of the system dynamics.

The first chapter gives a brief introduction to robot manipulators and the mechanical components of a manipulator arm. The issues involved in modeling a manipulator are discussed. Then a brief overview of the control schemes in the literature is given. In the second chapter, the modeling of a 2DOF Planar Manipulator is performed. The inverse kinematics equations are derived and the dynamic model is formulated using the Euler-Lagrange method. In Chapter 3, the independent joint control scheme is developed. For this purpose, each rotary joint of the manipulator is considered as an individual system and the control is applied to each joint on a motor-load basis. Various linear control strategies, such as PD and PID are developed first and applied to each joint of the manipulator. As a second method, a nonlinear model based controller, known as the proportional-derivative plus (PD+) controller, is designed for the system assuming the system dynamics of the system are known. Finally, a chattering free sliding mode controller (SMC) is developed for the system, which can provide robustness against model uncertainties and external disturbances and does not require knowledge about the

system model. The performance of the system for all the controllers is analyzed and compared in Chapter 4. Finally, Chapter 5 presents our conclusions and future directions of this study.

2. MODELING OF 2-DOF PLANAR ELBOW MANIPULATOR

2.1 Introduction

Accurate modeling is essential for the development of simulations, which help to study the behavior of a system in advance. A good system model is also crucial for the performance of all model-based control techniques. The modeling of a robotic system involves the formulation of kinematic models of the links, as well as the dynamic model of the whole system including the model of the joint actuators. This section presents the complete kinematic and dynamic modeling procedure of a robot arm, taking a 2-DOF planar elbow manipulator into consideration. A model of the joint actuator is also derived to be used in our simulations.

2.2 Direct Kinematics of 2-DOF Planar Elbow Manipulator

Prior to the derivation of the kinematic parameters and kinematic model, frames are placed at each link to facilitate the derivation of homogeneous transformations. The transformation between frame i and $(i-1)$ is represented by two rotations and two translations, which are defined in terms of Denavit - Hartenberg (D-H) parameters as below :

$$Tran(0,0,d)Rot(z,\theta)Tran(a,0,0)Rot(x,\alpha) \qquad (2.1)$$

The four D-H parameters are defined as follows:

θ_i is the joint angle from the x_{i-1} axis to the x_i axis about the z_{i-1} axis.

d_i is the distance from the origin of the $(i-1)$th frame to the intersection of the z_{i-1} axis with the x_i axis along the z_{i-1} axis.

α_i is the offset angle between the z_{i-1} axis to the z_i axis.

a_i is the offset distance from the intersection of the z_{i-1} axis with the x_i axis to the origin of the ith frame along the x_i axis.

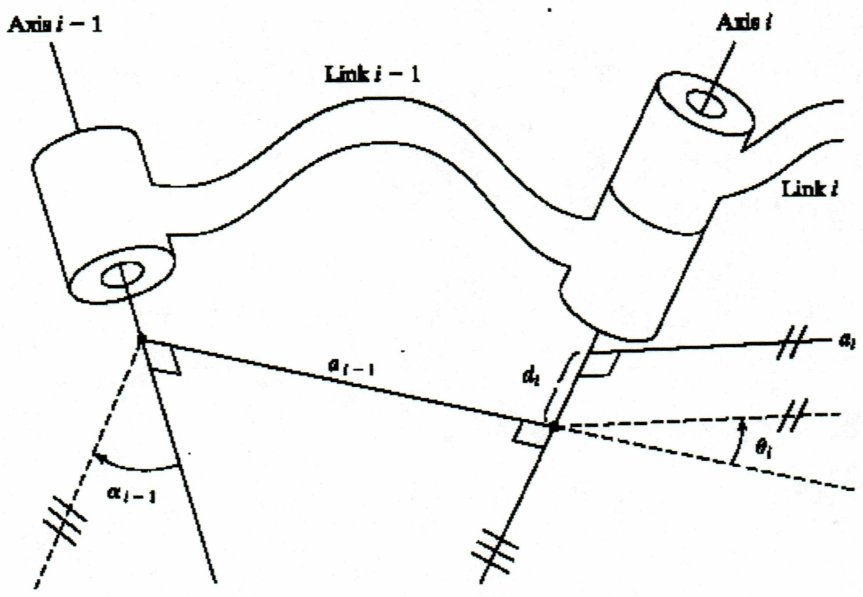

Fig. 2.1 Link connection description.

(Source: Craig, 1989)

These four parameters are used in the matrix description of the frame i with respect to the frame (i-1), as below;

$$A_i^{\,i-1} = \begin{bmatrix} \cos\theta_i & -\cos\alpha_i \sin\theta_i & \sin\alpha_i \sin\theta_i & a_i \cos\theta_i \\ \sin\theta_i & \cos\alpha_i \cos\theta_i & -\sin\alpha_i \cos\theta_i & a_i \sin\theta_i \\ 0 & \sin\alpha_i & \cos\alpha_i & d_i \\ 0 & 0 & 0 & 1 \end{bmatrix} \tag{2.2}$$

Now, using the above approach we will derive the kinematics of the 2-DOF planar elbow manipulator. For this purpose, we establish a frame at the base and at each adjacent link of the 2-DOF manipulator, as shown in Fig. 2.2.

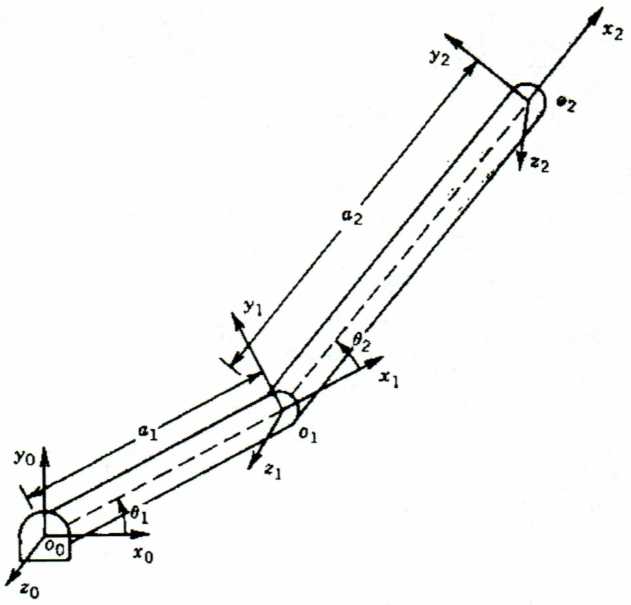

Fig. 2.2 Two link planar elbow manipulator

(Source: Spong and Vidyasagar, 1989)

The link parameters for the 2-DOF system are shown in Table 2.1.

Table 2.1 Link parameters of 2-DOF manipulator.

Link	a_i	α_i	d_i	θ_i
1	a_1	0	0	θ_1
2	a_2	0	0	θ_2

θ_1, θ_2 are variables.

The transformation matrices for each link are derived as below:

$$A_1 = \begin{bmatrix} \cos\theta_1 & -\sin\theta_1 & 0 & a_1\cos\theta_1 \\ \sin\theta_1 & \cos\theta_1 & 0 & a_1\sin\theta_1 \\ 0 & 0 & 1 & 0 \\ 0 & 0 & 0 & 1 \end{bmatrix} \tag{2.3}$$

$$A_2 = \begin{bmatrix} \cos\theta_2 & -\sin\theta_2 & 0 & a_2\cos\theta_2 \\ \sin\theta_2 & \cos\theta_2 & 0 & a_2\sin\theta_2 \\ 0 & 0 & 1 & 0 \\ 0 & 0 & 0 & 1 \end{bmatrix} \tag{2.4}$$

Thus, the transformation of the end-effector with respect to the base frame is derived by multiplying the two matrices A_1 and A_2:

$$A_0^2 = \begin{bmatrix} \cos(\theta_1+\theta_2) & -\sin(\theta_1+\theta_2) & 0 & a_1\cos\theta_1 + a_2\cos(\theta_1+\theta_2) \\ \sin(\theta_1+\theta_2) & \cos(\theta_1+\theta_2) & 0 & a_1\sin\theta_1 + a_2\sin(\theta_1+\theta_2) \\ 0 & 0 & 1 & 0 \\ 0 & 0 & 0 & 1 \end{bmatrix} \tag{2.5}$$

The first two terms of the last column of A_0^2 are the position coordinates (x, y) of the end-effector, while the 2 × 2 matrix in the upper left section gives the orientation of the end-effector with respect to the base frame.

2.3 Inverse Kinematics of 2-DOF Planar Elbow Manipulator

In the previous section, the end-effector coordinates x and y were derived with respect to given joint variables θ_1 and θ_2. However, robot control involves the generation of appropriate torques/forces for the point-by-point or tracking control of the joint displacements to achieve a desired position or trajectory of the end-effector. This requirement dictates the derivation of inverse kinematics, which describes joint displacements as a function of the end-effector coordinates. As discussed in the first chapter the solution for this problem may not be unique for the case of a 2-DOF planar elbow manipulator. If the given (x, y) coordinates are out of reach of the manipulator, then there may be no solution and if the coordinates (x, y) are within the reach of the

manipulator there may be two solutions, as shown in Fig. 2.2. These two configurations are so-called elbow up and elbow down configurations. There may be exactly one solution for this problem if the manipulator is to be fully extended to reach a point. Consider the diagram of Fig. 2.3.

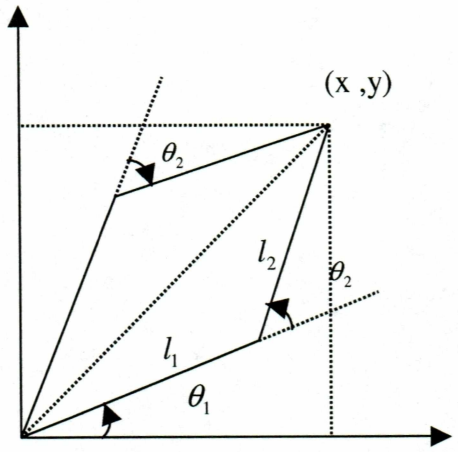

Fig. 2.3 Multiple inverse kinematic solutions.

Calculating angle θ_2 for the elbow down configuration,

$$x^2 + y^2 = l_1^2 + l_2^2 + 2l_1 l_2 \cos\theta_2 \tag{2.6}$$

$$\cos\theta_2 = \frac{x^2 + y^2 - l_1^2 - l_2^2}{2l_1 l_2} = B \tag{2.7}$$

We determine θ_2 as

$$\theta_2 = \cos^{-1}(B) \tag{2.8}$$

Sine of the angle θ_2 is given by

$$\sin(\theta_2) = \pm\sqrt{1 - B^2} \tag{2.9}$$

and, hence, θ_2 is found by

$$\theta_2 = \tan^{-1}\frac{\pm\sqrt{1 - B^2}}{B} \tag{2.10}$$

The above representation of angle θ_2 allows us to recover the elbow up and elbow down configurations by choosing the positive and negative signs in (2.10), respectively.

θ_1 is now given as

$$\theta_1 = \tan^{-1}(y/x) - \tan^{-1}\left(\frac{l_2 \sin\theta_2}{l_1 + l_2 \cos\theta_2}\right) \tag{2.11}$$

We can observe that angle θ_1 depends on θ_2, which makes sense as we would require different values for θ_1 depending on the solution chosen for θ_2.

2.4 Dynamics of 2-DOF Planar Elbow Manipulator

Due to the low number of DOF involved in the problem under consideration and the analytical description it offers, the Lagrange-Euler method is used to formulate the equations of motion of the 2-DOF manipulator. The method involves calculating the kinetic and potential energies of the manipulator and finally applying the Lagrangian formulation to derive the equations of motion. For simplicity, we assume the masses m_1 and m_2 to be point masses that exist at the distal end of each link, which will also allow reflecting the variation of load to the dynamic model in a very straightforward manner. Consider Fig. 2.4.

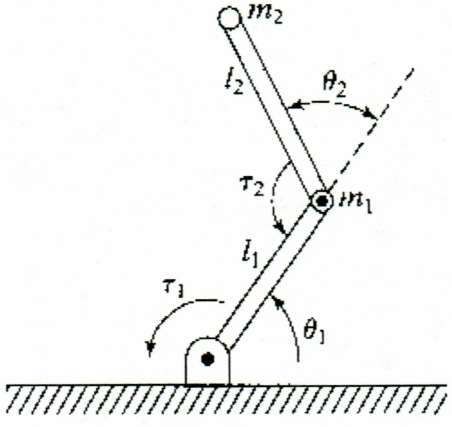

Fig. 2.4 Two link planar elbow manipulator with point masses at the distal ends of the links.

The Lagrangian function is given by

$$L = k - u \tag{2.12}$$

Where, k is the total kinetic energy of the arm, and

u is the total potential energy of the arm.

The corresponding equations of motion are derived using Lagrange's equations

$$\frac{d}{dt}\frac{\partial L}{\partial \dot{\Theta}} - \frac{\partial L}{\partial \Theta} = \tau \tag{2.13}$$

where

Θ = joint angles (θ_1, θ_2)

$\dot{\Theta}$ = joint velocities

τ = n × 1 vector of actuator torques

which result in the following equations;

$$\tau_1 = m_2 l_2^2(\ddot{\theta}_1 + \ddot{\theta}_2) + (m_1 + m_2) l_1^2 \ddot{\theta}_1 + m_2 l_1 l_2 c_2 (2\ddot{\theta}_1 + \ddot{\theta}_2) - m_2 l_1 l_2 s_2 \dot{\theta}_2^2 - 2m_2 l_1 l_2 s_2 \dot{\theta}_1 \dot{\theta}_2 + m_2 l_2 g c_{12} + (m_1 + m_2) l_1 g c_1 \tag{2.14}$$

$$\tau_2 = m_2 l_2^2(\ddot{\theta}_1 + \ddot{\theta}_2) + m_2 l_1 l_2 c_2 \ddot{\theta}_1 + m_2 l_2 s_2 \dot{\theta}_1^2 + m_2 l_2 g c_{12} \tag{2.15}$$

where, m_1 : Mass of link 1

m_2 : Mass of link 2

l_1 : Length of link 1

l_2 : Length of link 2

g : Acceleration due to gravity

θ_1 : Angle that link 1 makes with the horizontal

θ_2 : Angle that link 2 makes with link 1

τ_1 : Torque applied on link 1

τ_2 : Torque applied on link 2

The complete derivation of the dynamic model of the 2-DOF planar elbow manipulator is included in the Appendix.

2.5 Motor Model

A common actuator found in many industrial robots is the permanent magnet DC motor. The main physical phenomenon that causes a motor to generate a torque when current passes through the windings is given by

$$F = qV \times B \tag{2.16}$$

where q is the charge, moving with velocity V through a magnetic field B, giving rise to a force. The torque- producing ability of the motor is directly proportional to the armature current and the constant magnetic field in the air gap, which is given by the torque constant, k_t.

$$\tau_m = k_t i_a \tag{2.17}$$

Due to the rotation of the motor, a voltage develops across the armature. This back emf voltage is given by

$$v_b = k_b \dot{\theta}_m \tag{2.18}$$

where v_b is the back emf voltage generated, k_b is the back emf constant, and $\dot{\theta}_m$ is the rotational velocity of the motor.

Fig. 2.5 shows the circuit diagram of a DC motor. The major components are

v_a = armature voltage source

L_a = armature inductance

R_a = armature resistance

v_b = back emf voltage

i_a = armature current

θ_m = rotor position

τ_m = generated torque

τ_l = load torque

Φ = magnetic flux due to stator.

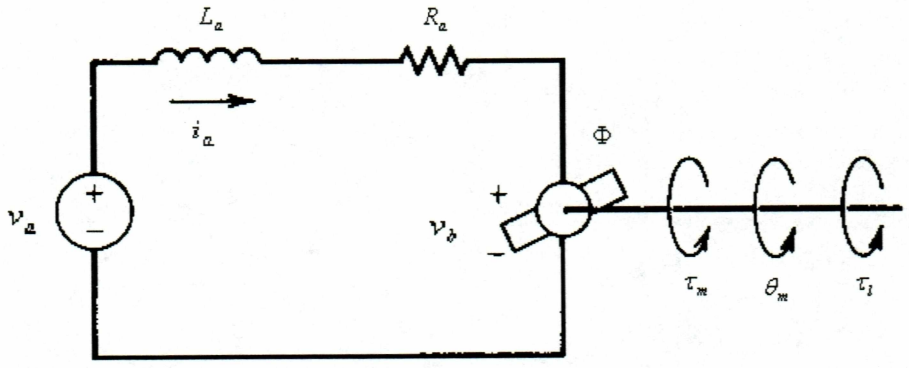

Fig. 2.5 Circuit diagram of a permanent magnet DC motor.

(Source: Spong and Vidyasagar, 1989)

The circuit is described by the first order differential equation:

$$L_a\dot{i}_a + R_a i_a = v_a - k_b\dot{\theta}_m \tag{2.19}$$

The mechanical part of the motor is shown in Fig. 2.6. The DC motor is connected to the link through a gear train with gear ratio $1:n$. We can observe from the figure that, J_m(motor inertia) is the sum of actuator and gear ratios. The equation of motion of this system is given by

$$\begin{aligned} J_m\ddot{\theta}_m + B_m\dot{\theta}_m &= \tau_m - n\tau_l \\ &= k_t i_a - n\tau_l \end{aligned} \tag{2.20}$$

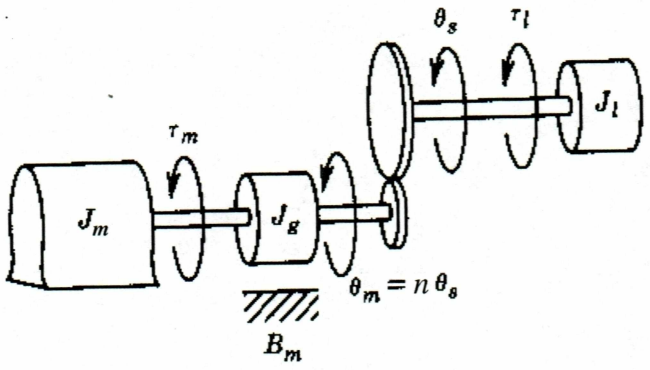

Fig. 2.6 Mechanical part of the DC motor with the load.

(Source: Spong and Vidyasagar, 1989)

The two equations (2.19) and (2.20) are converted into the Laplace domain and written as

$$(L_a s + R_a) I_a(s) = V_a(s) - k_b s \Theta_m(s) \tag{2.21}$$

$$(J_m s^2 + B_m s) \Theta_m(s) = k_t I_a(s) - n \tau_l(s) \tag{2.22}$$

The block diagram of the above system is shown in Fig. 2.7.

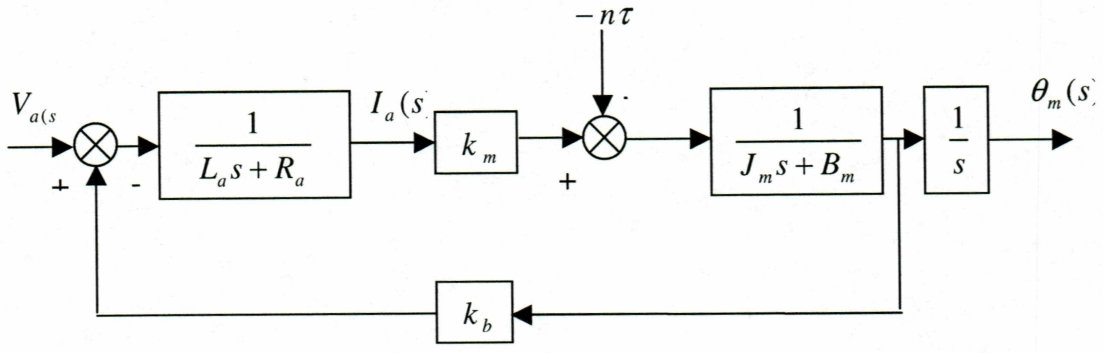

Fig. 2.7 Block diagram for permanent magnet DC motor.

2.6 Conclusion

The equations of motion derived for the two degree of freedom manipulator is a set of second order coupled nonlinear differential equations. It consists of the mass or inertia terms, coriolis and centrifugal forces between the joints, as well as terms reflecting the gravity effects. The torques/forces calculated are the functions of the manipulator physical parameters and instantaneous position, velocity, and acceleration values of the joints. The Lagrange-Euler method is favored for its simplicity in designing suitable control laws for a 2DOF manipulator. The motor model derived models a standard, commercially used motor in the industry of robots.

3. CONTROL OF 2-DOF PLANAR ELBOW MANIPULATOR

3.1 Introduction

Control methods in robotics can be classified by two basic approaches; independent joint control (IJC) and model based control (MBC). While the latter takes the full arm dynamic model into consideration in the design of the control input, the IJC approach considers each joint independently as a single-input-single-output system. With this approach, the robot control problem is converted to the problem of joint actuator control with arm dynamics taken into consideration as a disturbance. In this thesis, the independent joint control approach is taken for the development of the control techniques due to its modularity and tolerance for parameter and model uncertainties. The coupling and gravity effects due to the motion of other links are thus treated as disturbances.

The block diagram of the single input/single output system under consideration is shown in Fig. 3.1.

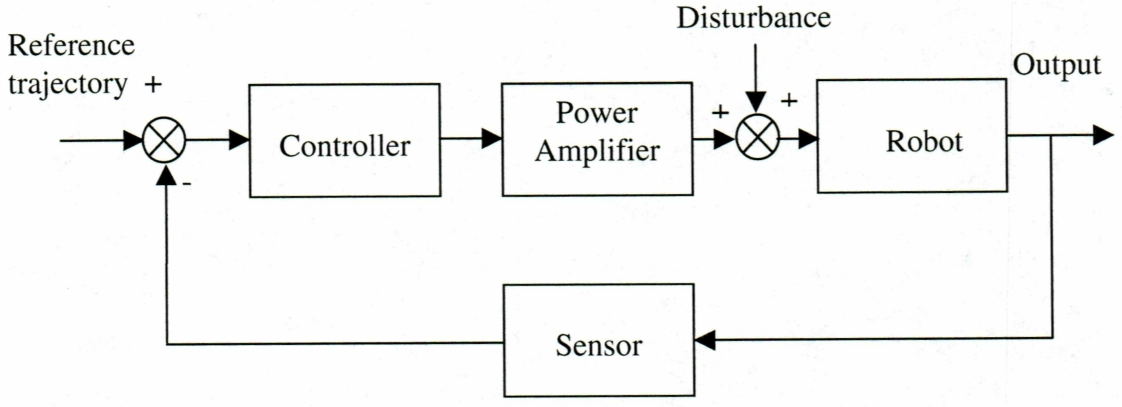

Fig. 3.1 Single input/single output feedback control system.

The basic aim of the control input is to make the plant follow a desired output for a given reference signal. However, the disturbance effects influencing the system performance should also be taken into consideration. Therefore, a controller must be

designed in such a way that the reference trajectory tracking is achieved, while also compensating for the effect of the disturbances acting on the system. Figs. 3.2 and 3.3 demonstrate the schematic diagrams of the 2-DOF closed-loop control system, also linking the PWM based switching strategy of the power converter. Thus, the diagrams also reflect the full dynamics that have been considered in the simulations.

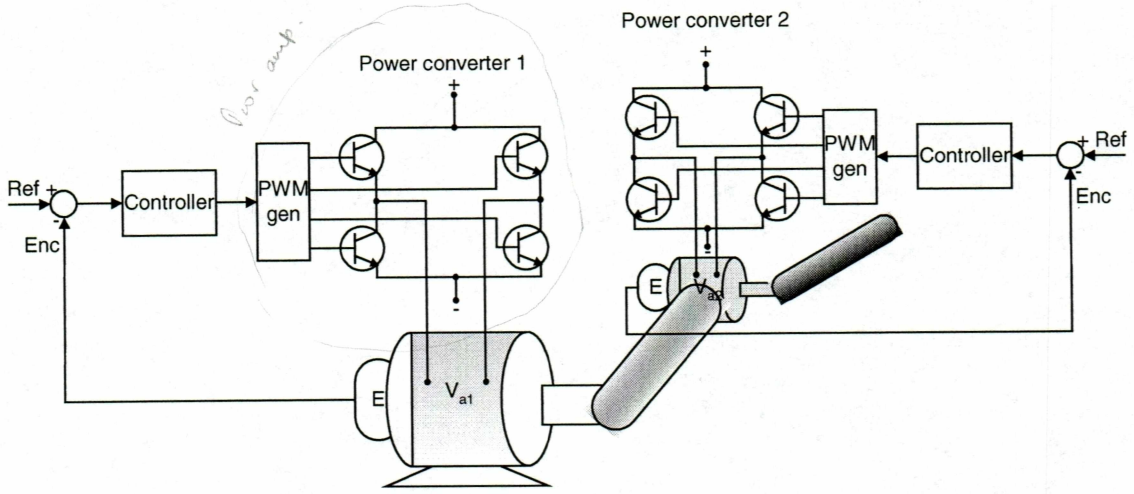

Fig. 3.2 Schematic of 2 DOF system with closed loop control.

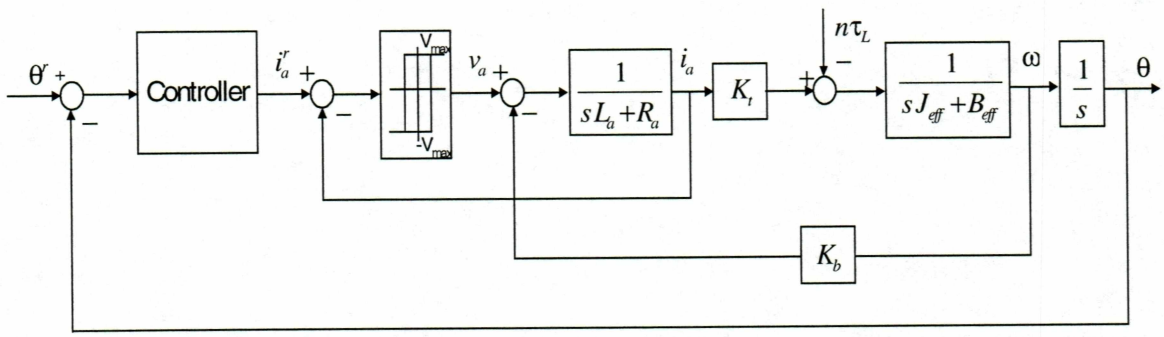

Fig. 3.3 Block diagram of feedback control.

3.2 Independent Joint PD Control

The equations of motion of an n-DOF planar manipulator can be written in the following general form:

$$M(\theta)\ddot{\theta}+C(\theta,\dot{\theta})\dot{\theta}+G(\theta)=\tau \ , \tag{3.1a}$$

with individual link dynamics given as;

$$\sum_{j=1}^{n} m_{jk}(\theta)\ddot{\theta}_j+\sum_{i,j=1}^{n} c_{ijk}(\theta)\dot{\theta}_i\dot{\theta}_j+g_k(\theta)=\tau_k \tag{3.1b}$$

On the other hand, the joint actuator model is given in the following form, neglecting the winding inductance, L_a:

$$J_m\ddot{\theta}_{m\,k}+(B_m+k_b k_m/R_a)\dot{\theta}_{mk}=k_m/R_a V_{ak}-n_k\tau_{lk} \tag{3.2}$$

where k = 1, …., n, dependent on the number of links. The equation (3.1) represents the motion of the manipulator that includes nonlinear inertial, centrifugal, coriolis, and gravitational effects and (3.2) represents the actuator dynamics. As can be seen in Fig. 3.2, τ_{lk}, which is the torque required for the dynamics of each link, is reflected as the disturbance effect on each joint actuator. This structure leads to the design of an independent controller for each joint as discussed in this section.

First, an independent joint PD control is developed as can be seen in Fig. 3.4.

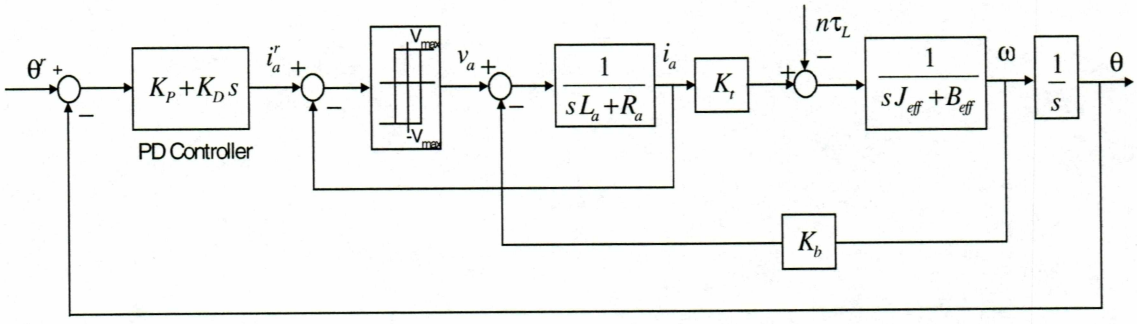

Fig. 3.4 Closed loop system with PD control.

Here, J_{eff} is the effective inertia, which includes the motor inertia and the linear inertial coefficients related to $\ddot{\theta}_j$ multiplied by the square of gear ratio n. B_{eff} is the effective friction, which is the sum of motor viscous friction and linear frictional terms of the load multiplied by the square of the gear ratio, n. The PWM switching procedure of the

current controller in the system is represented with a hysterisis function as can be seen in the diagram.

Thus, considering the 2-DOF planar robot arm, we design two PD controller inputs, one for each joint, in the following form:

$$u_1 = K_{P1}\, e_1 + K_{D1}\, \dot{e}_1 \tag{3.3a}$$

$$u_2 = K_{P2}\, e_2 + K_{D2}\, \dot{e}_2 \tag{3.3b}$$

Although the detailed dynamics given in Fig. 3.4 are taken into consideration for the simulations, for the control design process, the simplified version of the current control is taken into account. Based on the fast switching elements (IGBT's), an approximation of $i_a^r \approx i_a$ has been justified. Fig. 3.5 gives the simplified block diagram used in the control design.

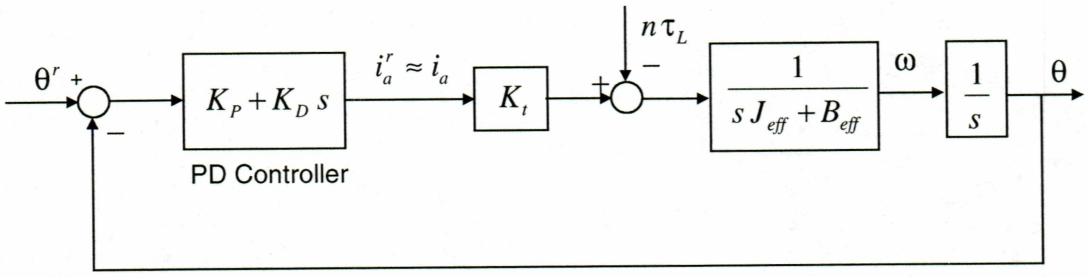

Fig. 3.5 Simplified version of closed loop PD control.

Using the above simplified model, the application of the PD control for each joint result in a transfer function $\frac{\theta(s)}{\theta^r(s)}$ as given below:

$$\frac{\theta(s)}{\theta^r(s)} = \frac{\dfrac{K_t\,(K_D\, s + K_P)}{J_{eff}}}{s^2 + s\dfrac{(B_{eff} + K_t\, K_D)}{J_{eff}} + \dfrac{K_t\, K_P}{J_{eff}}} \tag{3.4}$$

Analyzing the system in terms of ζ (damping ratio) and ω_n (undamped natural frequency),

$$\omega_n^2 = \frac{K_t K_P}{J_{eff}} \tag{3.5}$$

$$\zeta = \frac{B_{eff} + K_t K_D}{2\sqrt{K_t K_P J_{eff}}} \tag{3.6}$$

K_P is chosen such that it ensures:

$\omega_n \leq 0.5\omega_r$ (ω_r: lowest structural frequency in the system)

The boundary values on K_P and K_D are determined as follows [Bogosyan, 2004]:

$$0 < K_P \leq \frac{\omega_r^2 J_{eff}}{4K_t} \tag{3.7}$$

$$K_D \geq \frac{2\sqrt{K_t K_P J_{eff}} - B_{eff}}{K_t} \tag{3.8}$$

In this thesis, the determination of K_P and K_D is also performed by root locus analysis. For the PD based set-point position control, the reference position signal θ^r is compared to the actual position, θ, and the difference is multiplied by a proportional gain K_P to produce an output to the actuator. Additionally, the derivative gain K_D is multiplied with the actual velocity $\dot{\theta}$ (since $\dot{\theta}^r = 0$) to increase damping effects and ensure stability.

3.3 Independent Joint PID Control

As it is well-known, the PD control gives rise to a zero steady-state error for a step-type input, with Type 1 systems. Consequently, considering the fact that the position control of the joint actuator gives rise to a Type 1 system, the steady-state error would be zero for set-point position control. However, when the effect of link dynamics is also taken into account, a steady-state error, of

$$e_{\infty} \approx \frac{T_L}{K_P} \tag{3.9}$$

will occur. Thus, in the best case of constant disturbance (which is true in our set-point position control), the PD control will give rise to a constant steady-state error. As a solution, an integral term is added to the PD controller and thus, a PID (proportional-integral-derivative) controller is obtained. With integral control, the steady-state error due to step-type disturbances will be made zero. The input control for each joint can be given as below:

$$u_1(t) = K_{P1}\, e_1(t) + K_{D1}\, \dot{e}_1(t) + K_{I1} \int_0^t e_1(\tau)\, d\tau \tag{3.10}$$

$$U_1(s) = K_{P1}\, E_1(s) + K_{D1}\, s\, E_1(s) + \frac{K_{I1}}{s} E_1(s) \tag{3.11}$$

$$u_2(t) = K_{P2}\, e_2(t) + K_{D2}\, \dot{e}_2(t) + K_{I2} \int_0^t e_2(\tau)\, d\tau \tag{3.12}$$

$$U_2(s) = K_{P2}\, E_2(s) + K_{D2}\, s\, E_2(s) + \frac{K_{I2}}{s} E_2(s) \tag{3.13}$$

In this study, the determination of PID parameters is also performed by root locus analysis as will be presented in the result section. A PID controller is shown in Fig. 3.6.

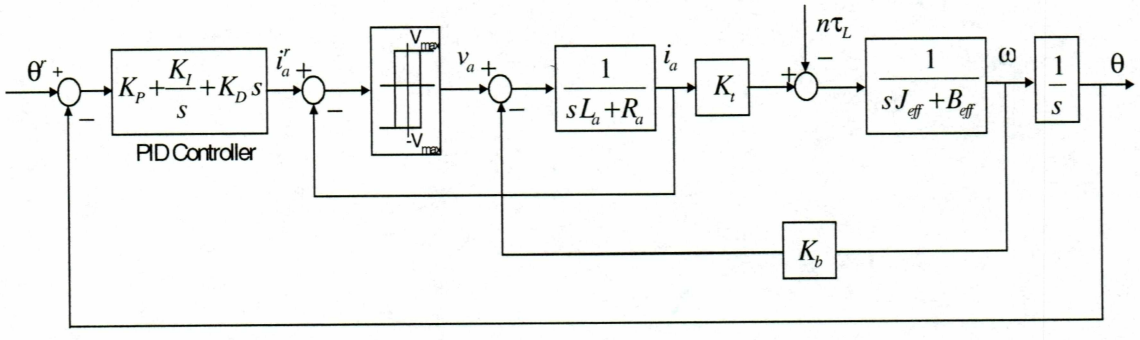

Fig. 3.6 Closed loop PID control.

3.4 Model-Based Controller (PD+)

A PD+ controller consists of a standard PD controller combined with the robot dynamics, which is assumed to be known. It has been proven that under exact robot and friction models and with the choice of symmetric positive definite matrices, K_P and K_D, the PD+ controller provides asymptotically exact tracking [Whitcomb, 1993].

The robot dynamics can be provided to the controller either by feedback or by feedforward terms. The advantage of using feedforward terms is that once the desired trajectory ($\theta_d, \dot{\theta}_d$ and $\ddot{\theta}_d$) for a given task has been satisfied, these terms can be computed off-line reducing the computational burden. However, with both feedback and feedforward control, the success of PD+ control is dependent on how well the system dynamics is known. Therefore, the schemes usually require an on-line parameter estimation method to compensate for parameter changes.

The closed loop system with PD+ control is shown in Fig. 3.7 for the 2-DOF robot arm.

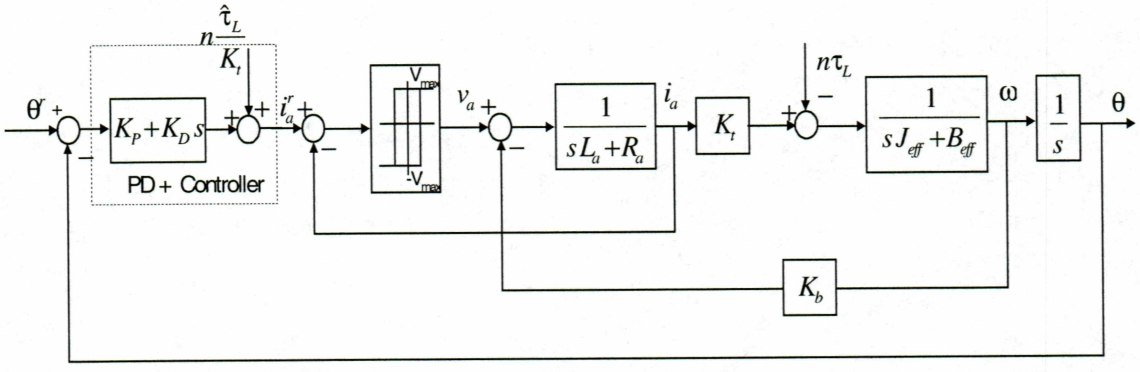

Fig. 3.7 Closed loop system with PD+ control.

For the system under consideration,

$$M(\theta)\ddot{\theta} + C(\theta,\dot{\theta})\dot{\theta} + G(\theta) = \tau \tag{3.14}$$

We can write the system model in the matrix form as below:

$$\begin{bmatrix} M_{11}+M_{11}(\theta_2) & M_{12}(\theta_2) \\ M_{12}(\theta_2) & M_{22} \end{bmatrix}\begin{bmatrix} \ddot{\theta}_1 \\ \ddot{\theta}_2 \end{bmatrix}+\begin{bmatrix} C_{11}(\theta_2)\dot{\theta}_2 & C_{12}(\theta_2)\dot{\theta}_2 \\ 0 & C_{22}(\theta_2)\dot{\theta}_2 \end{bmatrix}\begin{bmatrix} \dot{\theta}_1 \\ \dot{\theta}_2 \end{bmatrix}+$$

$$\begin{bmatrix} G_1(\theta_1,\theta_2) \\ G_2(\theta_1,\theta_2) \end{bmatrix}+\begin{bmatrix} B_{m1} & 0 \\ 0 & B_{m2} \end{bmatrix}\begin{bmatrix} \dot{\theta}_1 \\ \dot{\theta}_2 \end{bmatrix}=\begin{bmatrix} \tau_1 \\ \tau_2 \end{bmatrix} \tag{3.15}$$

where M_{11}, M_{12}, M_{22} are inertia terms; C_{11}, C_{12} and C_{22} are coriolis terms; G1 and G2 are gravitational terms, and finally, B_{m1} and B_{m2} are viscous friction coefficients of the link 1 and link 2. Separating the linear and nonlinear terms of inertia, the equation (3.15) can be written as;

$$\begin{bmatrix} M_{11} & 0 \\ 0 & M_{22} \end{bmatrix}\begin{bmatrix} \ddot{\theta}_1 \\ \ddot{\theta}_2 \end{bmatrix}+\begin{bmatrix} B_{m1} & 0 \\ 0 & B_{m2} \end{bmatrix}\begin{bmatrix} \dot{\theta}_1 \\ \dot{\theta}_2 \end{bmatrix}=\begin{bmatrix} \tau_1 \\ \tau_2 \end{bmatrix}-$$

$$\underbrace{\left\{\begin{bmatrix} M_{11}(\theta_2) & M_{12}(\theta_2) \\ M_{12}(\theta_2) & 0 \end{bmatrix}\begin{bmatrix} \ddot{\theta}_1 \\ \ddot{\theta}_2 \end{bmatrix}+\begin{bmatrix} C_{11}(\theta_2)\dot{\theta}_2 & C_{12}(\theta_2)\dot{\theta}_2 \\ 0 & C_{22}(\theta_2)\dot{\theta}_2 \end{bmatrix}\begin{bmatrix} \dot{\theta}_1 \\ \dot{\theta}_2 \end{bmatrix}+\begin{bmatrix} G_1(\theta_1,\theta_2) \\ G_2(\theta_1,\theta_2) \end{bmatrix}\right\}}_{\hat{\tau}_L} \tag{3.16}$$

For a given reference position θ^r, the PD+ current control input can be represented as;

$$u = K_P(\theta^r-\theta)+K_D(\dot{\theta}^r-\dot{\theta})+\frac{\hat{\tau}_L}{K_t} \tag{3.17}$$

where u is the control current input; $\hat{\tau}_L$ is the load torque; the symbol '^' represents the calculated value of the load torque and K_t is the motor torque constant. Now, we can write the control current inputs for each joint actuator:

$$u_1 = K_{P1}(\theta_1^r-\theta_1)+K_{D1}(\dot{\theta}_1^r-\dot{\theta}_1)+\frac{\hat{M}_{11}(\theta_2)\ddot{\theta}_1+\hat{M}_{12}(\theta_2)\ddot{\theta}_2+\hat{C}_{11}(\theta_2)\dot{\theta}_1\dot{\theta}_2+\hat{C}_{12}(\theta_2)\dot{\theta}_2^2+\hat{G}_1(\theta_1,\theta_2)}{K_{t1}} \tag{3.18}$$

$$u_2 = K_{P2}(\theta_2^r - \theta_2) + K_{D2}(\dot{\theta}_2^r - \dot{\theta}_2) + \frac{\hat{M}_{12}(\theta_2)\ddot{\theta}_1 + \hat{C}_{22}(\theta_2)\dot{\theta}_2^2 + \hat{G}_2(\theta_1, \theta_2)}{K_{t2}} \tag{3.19}$$

where $\hat{M}_{11}(\theta_2), \hat{M}_{12}(\theta_2), \hat{M}_{22}$, $\hat{C}_{11}(\theta_2), \hat{C}_{12}(\theta_2), \hat{C}_{22}(\theta_2), \hat{G}_1(\theta_1, \theta_2)$ and $\hat{G}_2(\theta_1, \theta_2)$ are calculated system parameters. Exact cancellation will take place if the system parameters are known accurately, in which case the motion equation of the system is simplified into a simple model consisting of inertia and friction terms only. Therefore, a basic PD controller will be sufficient to track reference input signals for each link. Otherwise, the system will have steady-state error and the transient performance will not be satisfactory.

3.5 Sliding Mode Control (SMC)

Sliding mode control is a robust control technique, finding a wide range of applications in robot control due to the robustness it provides against structured or unstructured uncertainties, without the need for a prior knowledge of the system model. The sliding mode control involves choosing a suitable manifold in state space, called the switching surface, which represents the desired error dynamic of the system. The control input is chosen in such a way that the trajectories are always directed towards this surface and once on the surface, the trajectories remain on the surface. In other words, the sliding condition is an invariant set which makes the system robust to dynamic uncertainties and the closed loop dynamics are completely governed by the equations which define the surface. Since the parameters defining the surface are chosen by the designer, the closed loop dynamics of the system will be independent of any fluctuations or disturbances in the parameters of the system and robustness is achieved. Fig. 3.8 represents a sliding surface and trajectories directed to it.

We start SMC design for a 2-DOF planar elbow manipulator by writing the system equations in state space representation:

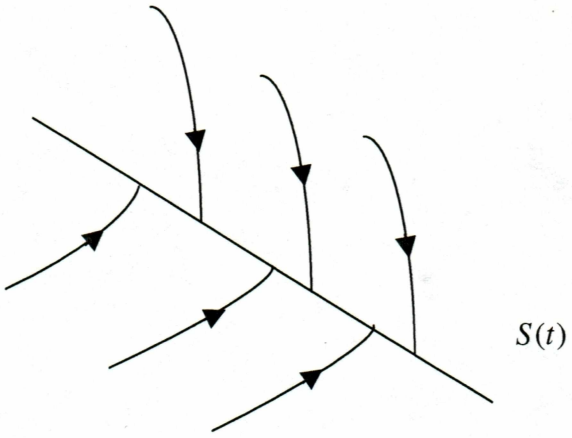

Fig. 3.8 Sliding surface.

$$\begin{bmatrix} \dot{\theta}_1 \\ \dot{\omega}_1 \\ \dot{\theta}_2 \\ \dot{\omega}_2 \end{bmatrix} = \begin{bmatrix} 0 & 1 & 0 & 0 \\ 0 & \dfrac{-B_{m1}}{m_2 l_2^2 + (m_1 + m_2) l_1^2 + I_{m1}} & 0 & 0 \\ 0 & 0 & 0 & 1 \\ 0 & 0 & 0 & \dfrac{-B_{m2}}{m_2 l_2^2 + I_{m2}} \end{bmatrix} \begin{bmatrix} \theta_1 \\ \omega_1 \\ \theta_2 \\ \omega_2 \end{bmatrix} +$$

$$\begin{bmatrix} 0 & 0 \\ \dfrac{1}{m_2 l_2^2 + (m_1 + m_2) l_1^2 + I_{m1}} & 0 \\ 0 & 0 \\ 0 & \dfrac{1}{m_2 l_2^2 + I_{m2}} \end{bmatrix} \begin{bmatrix} \tau_1 \\ \tau_2 \end{bmatrix} + \begin{bmatrix} 0 & 0 \\ \dfrac{-1}{m_2 l_2^2 + (m_1 + m_2) l_1^2 + I_{m1}} & 0 \\ 0 & 0 \\ 0 & \dfrac{-1}{m_2 l_2^2 + I_{m2}} \end{bmatrix} \begin{bmatrix} w_1 \\ w_2 \end{bmatrix} \tag{3.20}$$

where

$$w_1 = m_2 l_2^2 \ddot{\theta}_2 + m_2 l_1 l_2 c_2 (2\ddot{\theta}_1 + \ddot{\theta}_2) - m_2 l_1 l_2 s_2 \dot{\theta}_2^2 - 2 m_2 l_1 l_2 s_2 \dot{\theta}_1 \dot{\theta}_2 + m_2 l_2 g c_{12} + (m_1 + m_2) l_1 g c_1$$

$$w_2 = m_2 l_2^2 \ddot{\theta}_1 + m_2 l_1 l_2 c_2 \ddot{\theta}_1 + m_2 l_2 s_2 \dot{\theta}_1^2 + m_2 l_2 g c_{12}$$

Separating the two equations of motion, we have the first equation as

$$\dot{X}_1 = A_1 X_1 + B_1 u_1 - B_1 w_1 \tag{3.21}$$

which can be written as below in matrix form:

$$\begin{bmatrix} \dot{\theta}_1 \\ \dot{\omega}_1 \end{bmatrix} = \begin{bmatrix} 0 & 1 \\ 0 & a_{22} \end{bmatrix} \begin{bmatrix} \theta_1 \\ \omega_1 \end{bmatrix} + \begin{bmatrix} 0 \\ b_{21} \end{bmatrix} \tau_1 - \begin{bmatrix} 0 \\ b_{21} \end{bmatrix} w_1$$

The second equation of motion is given by

$$\dot{X}_2 = A_2 X_2 + B_2 u_2 - B_2 w_2 \tag{3.22}$$

and in matrix form,

$$\begin{bmatrix} \dot{\theta}_2 \\ \dot{\omega}_2 \end{bmatrix} = \begin{bmatrix} 0 & 1 \\ 0 & a_{44} \end{bmatrix} \begin{bmatrix} \theta_2 \\ \omega_2 \end{bmatrix} + \begin{bmatrix} 0 \\ b_{42} \end{bmatrix} \tau_2 - \begin{bmatrix} 0 \\ b_{42} \end{bmatrix} w_2$$

Now we define a time-varying surface $\sigma(t)$ in the state-space as

$$\sigma(t) = \begin{bmatrix} \sigma_1(t) \\ \sigma_2(t) \end{bmatrix} = \begin{bmatrix} \dot{e}_1 + c_1 e_1 \\ \dot{e}_2 + c_2 e_2 \end{bmatrix} \tag{3.23}$$

with $\sigma_1(t)$ and $\sigma_2(t)$, for link 1 and link 2, respectively.

Here, $e_1 = \theta_1^r - \theta_1$

$e_2 = \theta_2^r - \theta_2$

in which θ_1^r, θ_2^r represents the position references for each joint, while θ_1 and θ_2 are the actual angular positions of the joints. We choose the design parameters c_1 and c_2, for the desired error dynamics for each link.

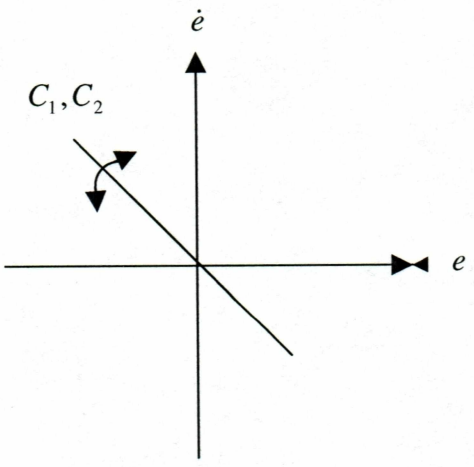

Fig. 3.9 Sliding condition.

Here, the problem of tracking $\theta \equiv \theta^r$ is equivalent to that of remaining on the surface $\sigma(t)$ for all $t > 0$. To ensure the stability of the error dynamics, a Lyapunov function is selected:

$$V = \frac{1}{2}\sigma^T \sigma \quad > 0 \tag{3.24}$$

The derivative of the above equation should be negative definite:

$$\dot{V} \leq 0$$

in other words, it should be equal to zero only when $e = \dot{e} = 0$ and negative, otherwise. For this purpose, we propose

$$\dot{V} = \sigma^T \dot{\sigma} \quad = \quad -\sigma^T D\sigma \quad < 0 \tag{3.25}$$

where D is a positive definite matrix.

$$D = \begin{bmatrix} d_1 & 0 \\ 0 & d_2 \end{bmatrix}$$

$$\sigma = \begin{bmatrix} \sigma_1 \\ \sigma_2 \end{bmatrix}$$

Canceling the common term σ^T on both sides of equation (3.25) we have

$$\dot{\sigma} + D\sigma = 0 \tag{3.26}$$

$$\begin{bmatrix} \ddot{e}_1 + c_1 \dot{e}_1 \\ \ddot{e}_2 + c_2 \dot{e}_2 \end{bmatrix} + \begin{bmatrix} d_1 & 0 \\ 0 & d_2 \end{bmatrix} \begin{bmatrix} \dot{e}_1 + c_1 e_1 \\ \dot{e}_2 + c_2 e_2 \end{bmatrix} = 0$$

The error equations are identical and only differ by different values for design parameters.

Consider the first equation represented by the above state space representation:

$$\ddot{e}_1 + c_1 \dot{e}_1 + d_1 (\dot{e}_1 + c_1 e_1) = 0 \tag{3.27}$$

Here $\ddot{e}_1 = \dot{\omega}_1^r - \dot{\omega}_1$; $\dot{\omega}_1^r$ and $\dot{\omega}_1$ are the reference and actual derivatives of angular velocities, respectively.

Substituting the expression for $\dot{\omega}_1$ from (3.21) for $\dot{\sigma}$, we have

$$\dot{\sigma}_1 = \dot{\omega}_1^r - a_{22}\,\omega_1 + b_{21}\,\tau_1 + b_{21}\,w_1 \tag{3.28a}$$

At this point, we should find and input torque value that would make $\dot{\sigma}_1 = 0$. This is called for equivalent control τ_{eq1}, which is the desired torque value to keep the dynamics of link 1 on the selected sliding surface.

$$\tau_{eq1} = \frac{\dot{\omega}_1^r - a_{22}\,\omega_1 + b_{21}\,w_1}{b_{21}} \tag{3.29b}$$

From equation (3.28a), the following expression is obtained for $\dot{\sigma}_1$:

$$\dot{\sigma}_1 = b_{21}\,(\tau_{eq1} - \tau_1) \tag{3.30}$$

$$b_{21}\,(\tau_{eq1} - \tau_1) + d_1\,\sigma_1 = 0 \tag{3.31}$$

Discretizing (3.30) and (3.31), we have

$$\frac{\sigma_1(k) - \sigma_1(k-1)}{T} = b_{21}\,(\tau_{eq1}(k-1) - \tau_1(k-1)) \tag{3.32}$$

$$b_{21}\,(\tau_{eq1}(k) - \tau_1(k)) + d_1\,\sigma_1(k) = 0 \tag{3.33}$$

Solving for $\tau_{eq1}(k-1)$ and $\tau_{eq1}(k)$ from (3.32) and (3.33), we have

$$\tau_{eq1}(k-1) = \tau_1(k-1) + \frac{\sigma_1(k) - \sigma(k-1)}{b_{21}\,T} \tag{3.34}$$

$$\tau_{eq1}(k) = \tau_1(k) - \frac{d_1}{b_{21}}\sigma_1(k) \tag{3.35}$$

At this point, we can assume the equivalent control is an average control and it would not change in one period, i.e,

$$\tau_{eq1}(k-1) = \tau_{eq1}(k) \tag{3.36}$$

Finally, manipulating (3.24) and (3.25), we derive the governing equation for the torque input for link 1,

$$\tau_1(k) = \tau_1(k-1) + \frac{1}{b_{21}T}[(1+d_1T)\sigma_1(k) - \sigma_1(k-1) \tag{3.37}$$

and link 2,

$$\tau_2(k) = \tau_2(k-1) + \frac{1}{b_{42}T}[(1+d_2T)\sigma_2(k) - \sigma_2(k-1) \tag{3.38}$$

3.6 Conclusion

In this chapter, various controllers are designed for the 2-DOF planar robot arm. The controllers, namely, PD, PID, PD+ and SMC, are developed and implemented based on the independent joint control, in which the control problem is converted to the problem of joint actuator control. The arm dynamics and load variations are seen by the controllers as disturbances. The PD and PID controllers are linear controllers and are still widely used in the robot industry due to their ease of application. PD control will result in a steady-state error under disturbance effects, while PID will make the steady-state error zero for step type disturbances only. Therefore, for more sophisticated applications, PD+ controllers appear to be more effective, provided an accurate knowledge of the model is available. However, even with a good amount of a priori information, parameter and load variations will give rise to tracking errors. Thus, for a good performance under any conditions, PD+ controllers must be combined with on-line parameter adaptation techniques. The SMC method, on other hand, does not require an accurate knowledge of

the model and system dynamics and will exhibit robustness to the external disturbances and inaccuracies in system dynamics.

4. SIMULATION RESULTS

4.1 Introduction

To evaluate the performance of the developed control methods, realistic simulation models are developed for both geared and direct-drive type 2-DOF planar manipulators. The PD, PID, PD+ and SM controllers are tested via simulations on the developed models under unknown load variations. In this section, the controller results will be presented for the geared type 2-DOF planar arm. Below is a list of the system parameters taken into consideration for the geared system.

$m_1 = 0.75$ kg

$m_2 = 0.2$ kg

$l_1 = 0.4$ m

$l_2 = 0.2$ m

$g = 9.81$ m/s^2

The motor1 parameters are:

$R_1 = 2$ Ohms

$L_1 = 0.02$ H

$K_{t1} = K_{b1} = 0.3$ Nm/A

Gear ratio $n_1 = 60$

$I_{m1} = 0.012$ kg.m^2

$B_{m1} = 0.006$ Nm.s/rad

The motor2 parameters are:

$R_2 = 2$ Ohms

$L_2 = 0.02$ H

$K_{t2} = K_{b2} = 0.3$ Nm/A

Gear ratio $n_2 = 60$

$I_{m2} = 0.012\,\text{kg.m}^2$

$B_{m2} = 0.006$ Nm.s/rad

4.2 Determination of PD Design Parameters

The K_P and K_D parameters of the PD controller are determined using root locus analysis. For this purpose, the detailed system taken into consideration as the system model for simulations is simplified as given in Fig. 3.5. Here, the actual actuator winding current i_a is assumed to be equal to the reference current i_a^r. Thus, nonlinearities related to the PWM switching procedure are neglected for the root locus analysis. The arm dynamics acting as disturbance is also taken to be zero. Also, the electrical time constant (L/R) is assumed to be much smaller than the mechanical time constant (J_m/B_m) resulting in the open loop transfer function for the first motor as below;

$$\frac{\theta(s)}{\theta^{ref}(s)} = \frac{K_{t1}\, n_1}{s(s((m_2 l_2^2 + (m_1 + m_2) l_1^2)/n_1^2) + I_{m1}) + B_{m1})}$$

$$\frac{\theta(s)}{\theta^{ref}(s)} = \frac{18}{0.012s^2 + 0.207s}$$

To have a common performance both with the geared and direct-drive system, a transient performance with 5% overshoot and a settling time of 0.4 sec is chosen. For this purpose, a single zero is added to the system open loop transfer function so that the root locus goes through the design point and achieves the desired transient response. The compensator zero for the motor1 is found to be -74.63 and the gain required is 0.18. The compensated root locus and system response are shown in Fig. 4.1 and 4.2, respectively. The proportional and derivative gains are:

$K_{P1} = 13.43$

$K_{D1} = 0.18$

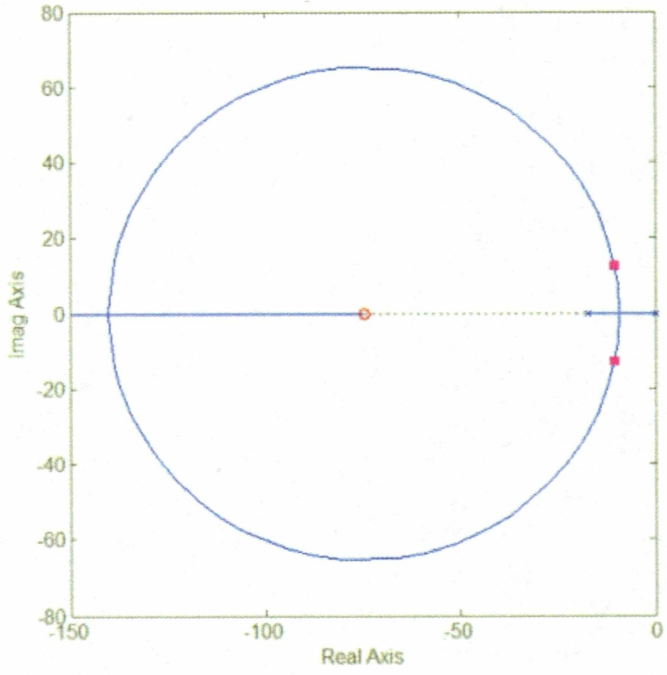

Fig. 4.1 Compensated root locus for motor1.

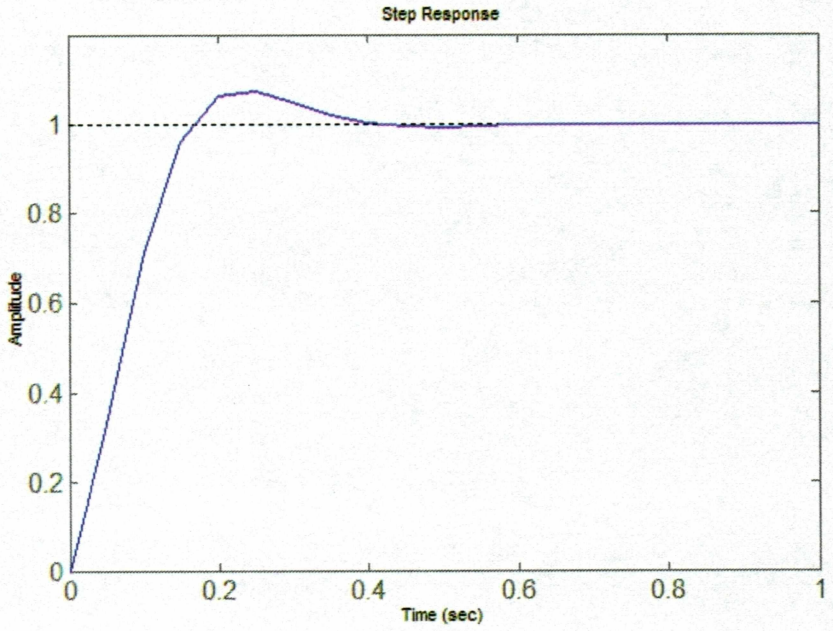

Fig. 4.2 Step response of the PD compensated system (motor1).

The open-loop transfer function for motor 2 is derived as below:

$$\frac{\theta(s)}{\theta^{ref}(s)} = \frac{K_{t2}\, n_2}{s(s((m_2 l_2^2)/n_2^2) + I_{m2}) + B_{m2})}$$

$$\frac{\theta(s)}{\theta^{ref}(s)} = \frac{18}{0.006s^2 + 0.1s}$$

With the application of root locus analysis in a similar manner to link 2, the following design parameters are obtained:

$K_{P2} = 8.91 \;\; K_{D2} = 0.13$

Similarly, the compensator gains for the direct-drive system are calculated and given by:

$K_{P1} = 18.61 \;\; K_{D1} = 7.16$

$K_{P2} = 14.11 \;\; K_{D2} = 2.88$

4.3 Determination of PID Design Parameters

As is well known, PD will result in a steady state error with constant disturbance effects. To improve the steady state response of the system, a pole and extra zero very close to the origin are selected for the PI compensator. This results in a PID controller. The transfer function of the additional PI compensator is chosen as

$$G_I(s) = \frac{s + 0.1}{s}$$

The compensator gains for the first motor are:

$K_{P1} = 13.43 \; K_{D1} = 0.18 \;\; K_{I1} = 1.38$

The compensator gains for the second motor are:

$K_{P2} = 8.91 \;\; K_{D2} = 0.13 \; K_{I2} = 0.81$

For the direct-drive system, the compensator gains are:

$K_{P1} = 18.61 \;\; K_{D1} = 7.16 \; K_{I1} = 1.85$

$K_{P2} = 14.11 \;\; K_{D2} = 2.88 \; K_{I2} = 1.38$

4.4 Simulation Results of the Geared System with PD Control

All simulations were carried out under the following initial conditions of the robot arm:

$\theta_1(0) = \theta_2(0) = 0$; $\omega_1(0) = \omega_2(0) = 0$

θ_1, θ_2 : Angular positions of link 1 and link 2, respectively.

ω_1, ω_2 : Angular velocities of link1 and link 2, respectively.

First, simulations are performed for a step-type joint reference and for payloads of $m_2 = 0.2\,\text{kg}$ and $m_2 = 0.4\,\text{kg}$. The determination of the PD parameters has been performed for $m_2 = 0.2\,\text{kg}$. Figs. 4.3 and 4.4 represent the variation of angular positions, Figs. 4.5 and 4.6 depict the variation of tracking errors, and the Fig. 4.7 demonstrates the angular velocity of both the motors.

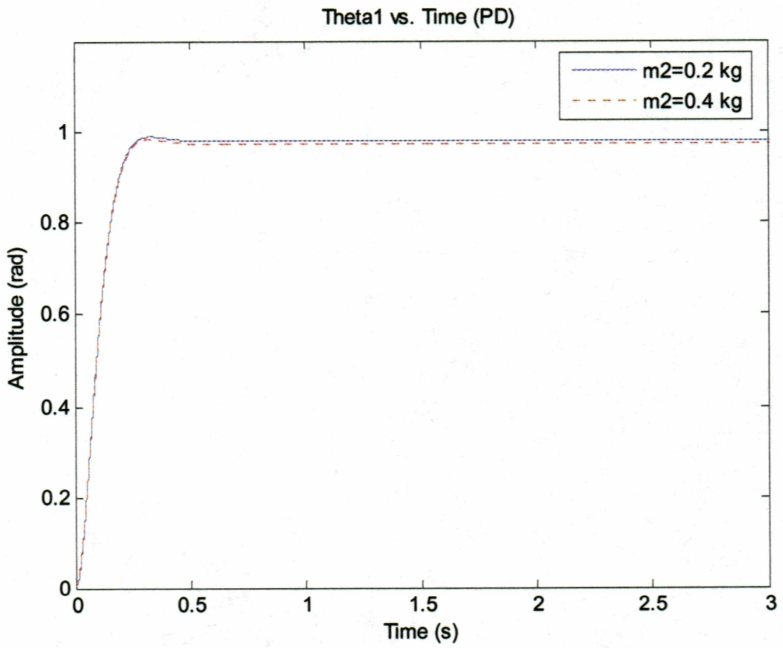

Fig. 4.3 Variation of angular position1 with change in the payload under PD control.

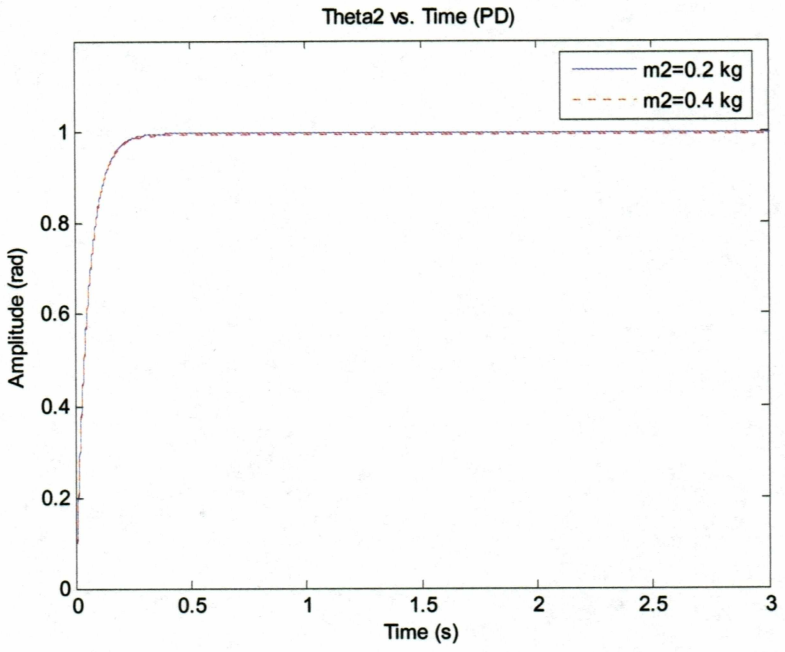

Fig. 4.4 Variation of angular position2 with change in the payload under PD control.

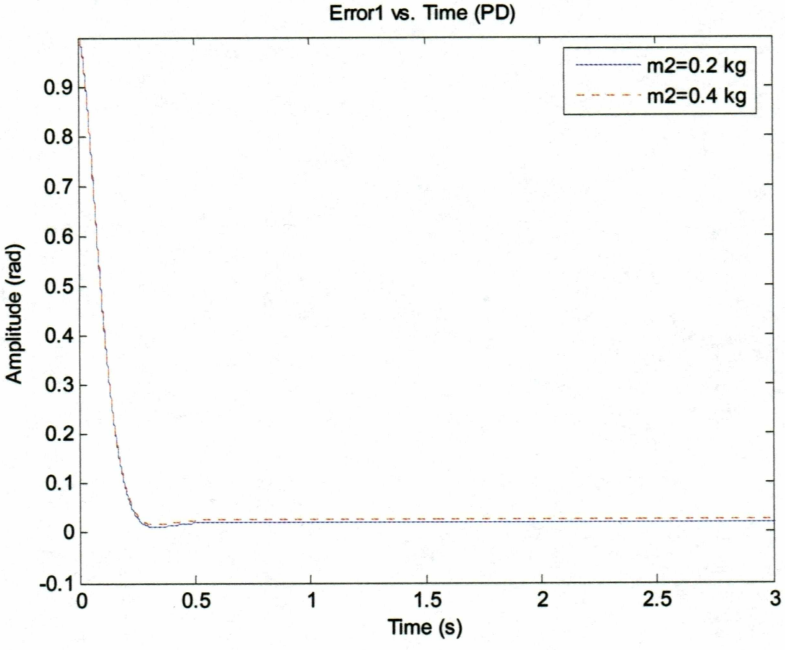

Fig. 4.5 Variation of tracking error1 with change in the payload under PD control.

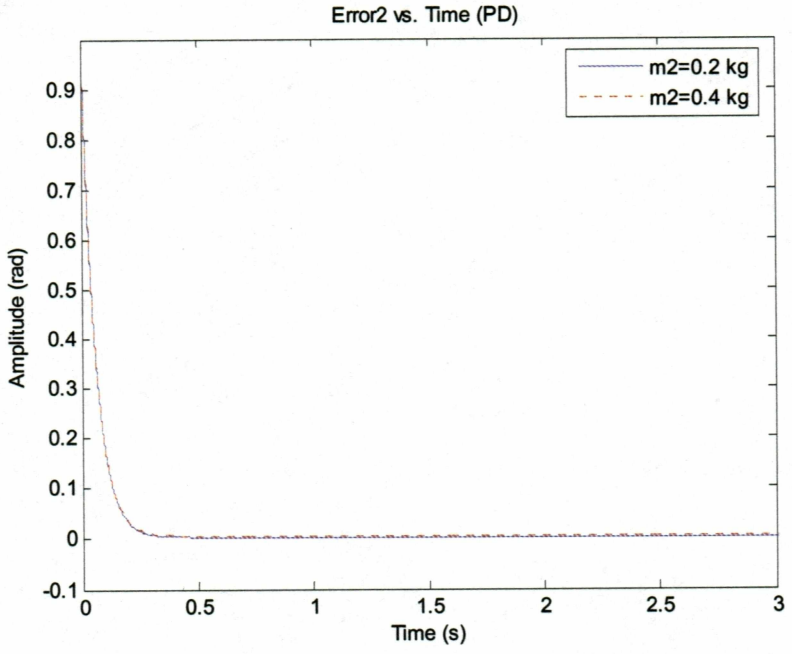

Fig. 4.6 Variation of tracking error 2 with change in the payload under PD control.

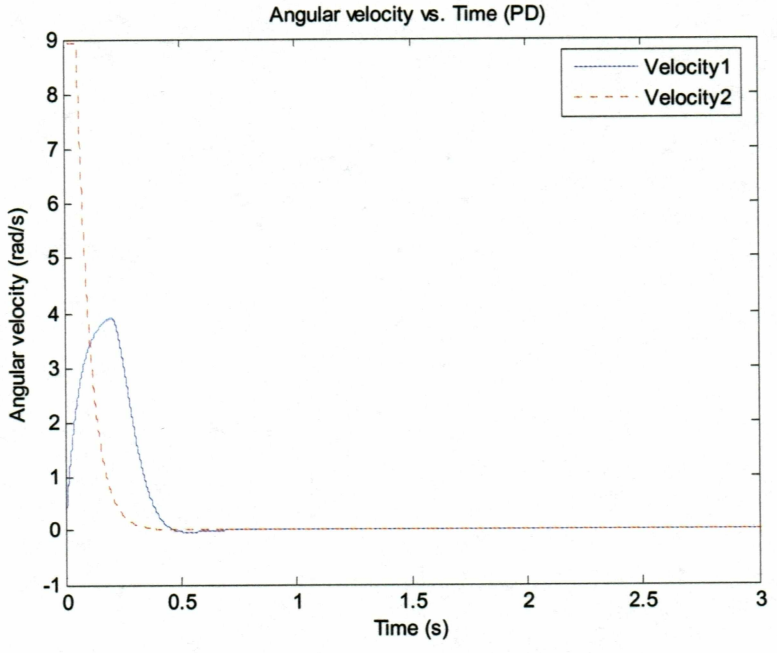

Fig. 4.7 Angular velocities of both motors under PD control.

The plots indicate that for a step-type reference, there is a constant steady state error which increases when the mass of the second arm is doubled. The resulting steady state errors for theta1 are 0.02 and 0.03, and for theta2, 0.027 and 0.052. The angular velocity plot indicates the expected result for set-point control which takes place with step inputs. The currents consumed by the motors to hold the arms of the robot at the desired positions are 24 mA and 13 mA. Figs. 4.10 and 4.11 show the variation of current of the two motors.

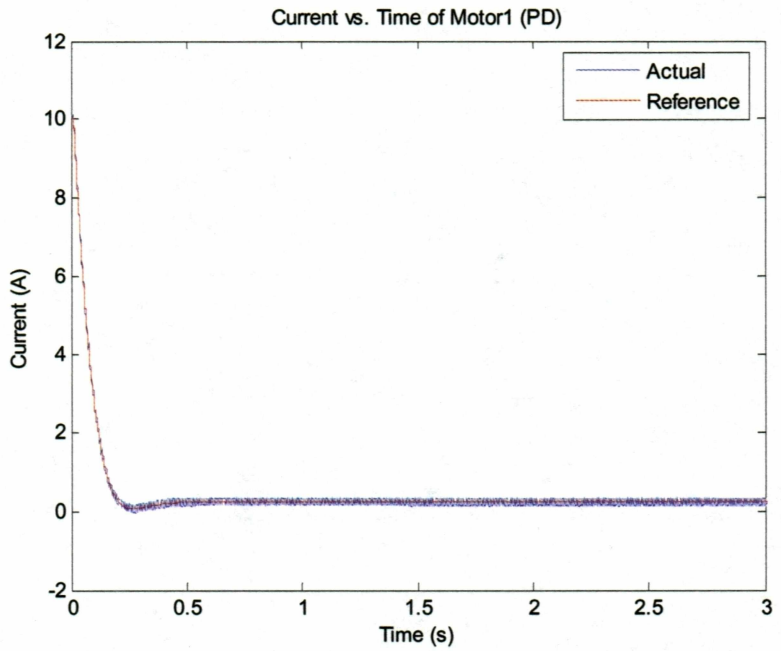

Fig. 4.8 Current variation of motor1.

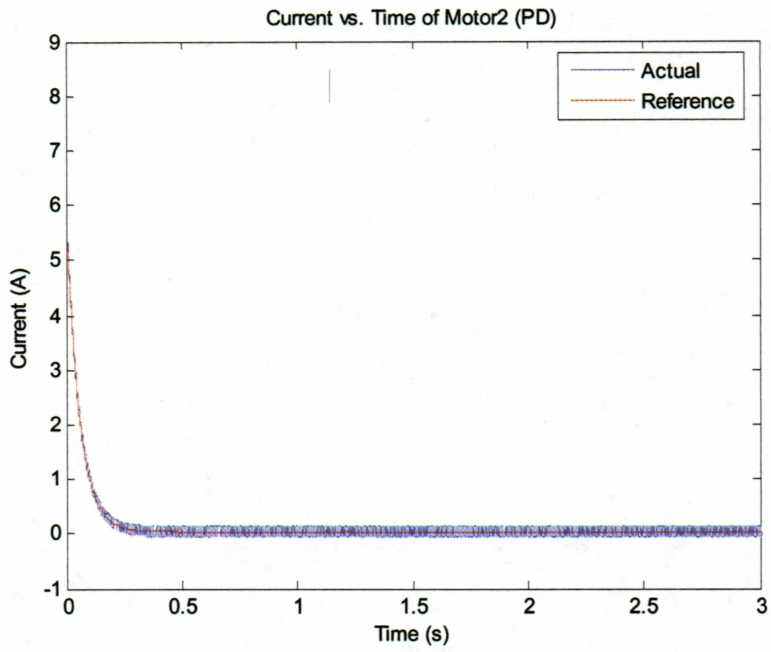

Fig. 4.9 Current variation of motor2.

4.5 Simulation Results of the Geared System with PID Control

A unit step is applied as the reference to both joints and the simulations are conducted with $m_2 = 0.2\,\text{kg}$ and $m_2 = 0.4\,\text{kg}$. The gains obtained by the root locus analysis of PID control for $m_2 = 0.2\,\text{kg}$ are used in the simulations. Figs. 4.10 and 4.11 represent the variation of angular positions, Figs. 4.12 and 4.13 depict the variation of tracking errors, and Fig. 4.14 shows the angular velocity of both links. The angular position of link 1 has a steady state error of 0.016. However, this error will reduce to zero if the simulation time is extended. This is expected due to the fact that PID control makes the steady-state error zero for constant disturbance effects, which is the case for the system with set-point control (step-type reference). As a matter of fact, the steady state error is observed to go to zero for the second link in a shorter time due to its smaller inertia. Once again the angular velocities have reached zero at steady state as expected with step-type references.

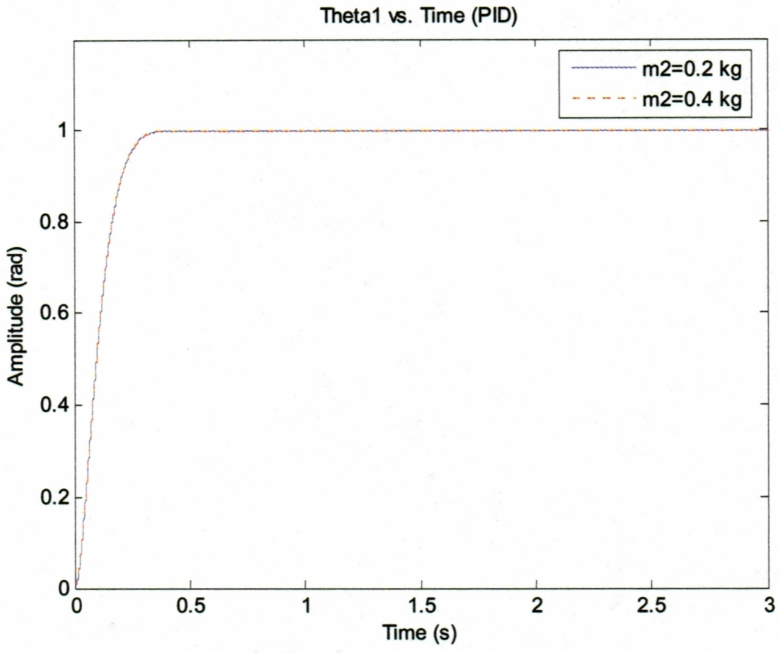

Fig. 4.10 Variation of angular position1 with change in the payload under PID control.

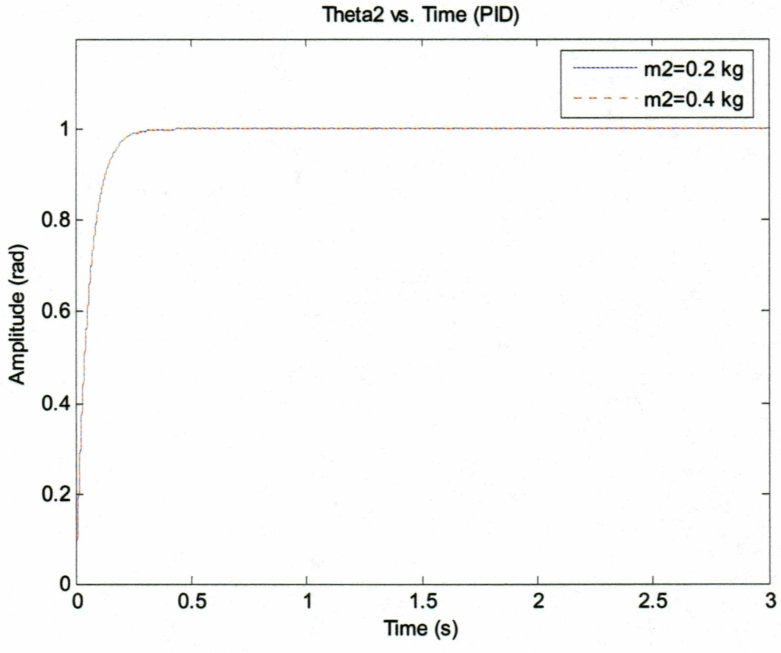

Fig. 4.11 Variation of angular position2 with change in the payload under PID control.

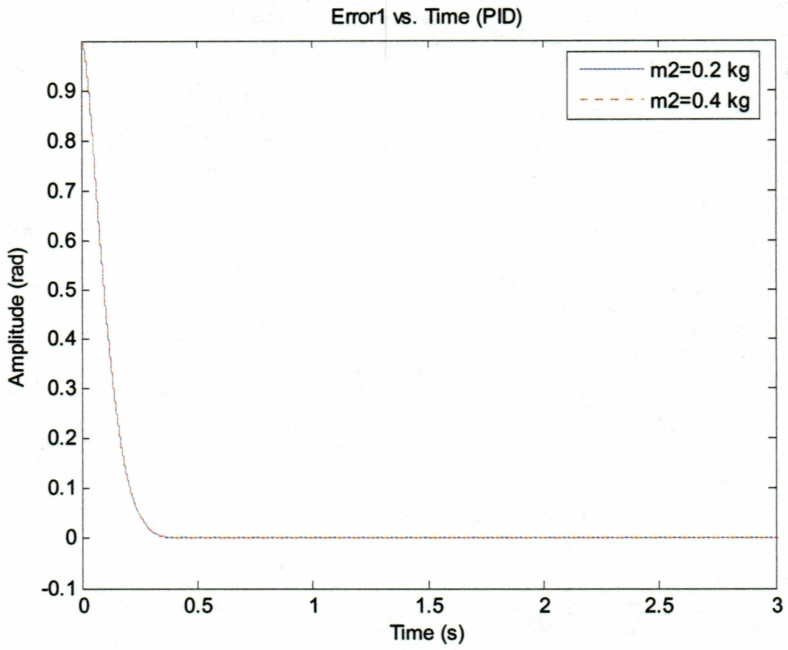

Fig. 4.12 Variation of tracking error1 with change in the payload under PID control.

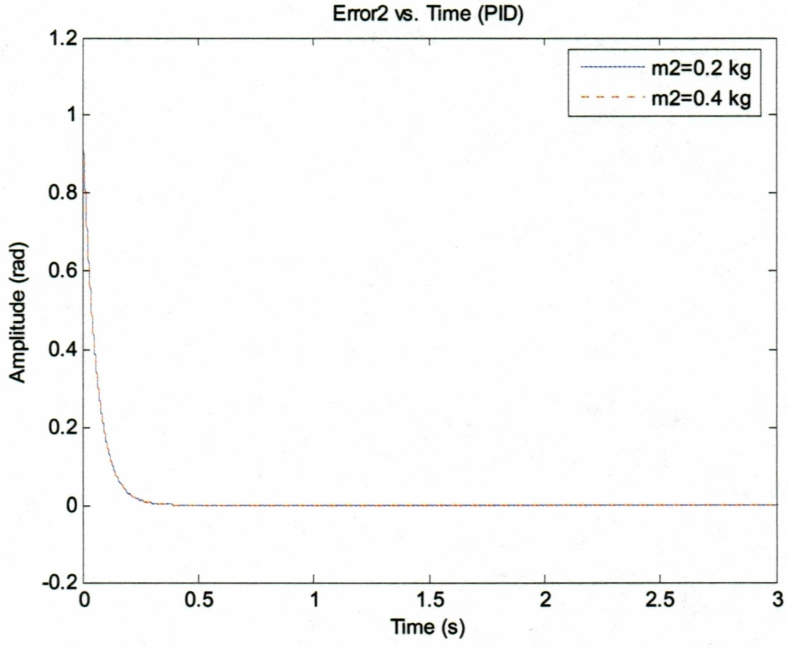

Fig. 4.13 Variation of tracking error2 with change in the payload under PID control.

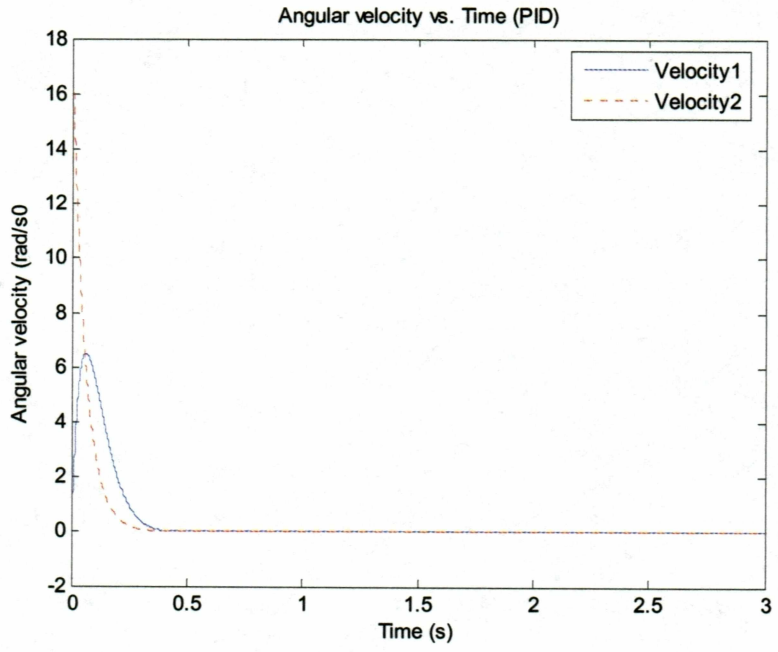

Fig. 4.14 Angular velocities of both motors under PID control.

Figs. 4.17 and 4.18 show the variation of current for the two motors. The current consumed by the motors to hold the links of the robot at the desired positions are 17 mA and 4 mA, respectively.

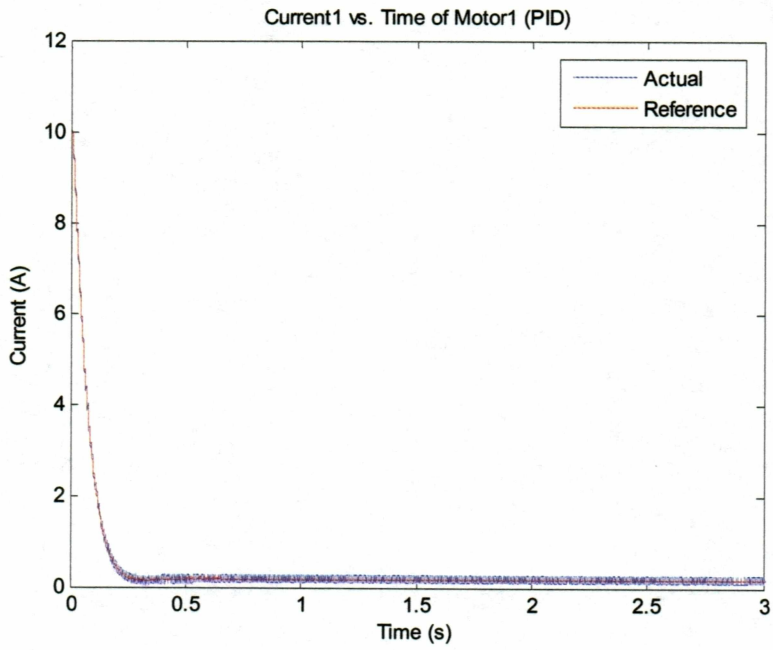

Fig. 4.15 Current variation of motor1.

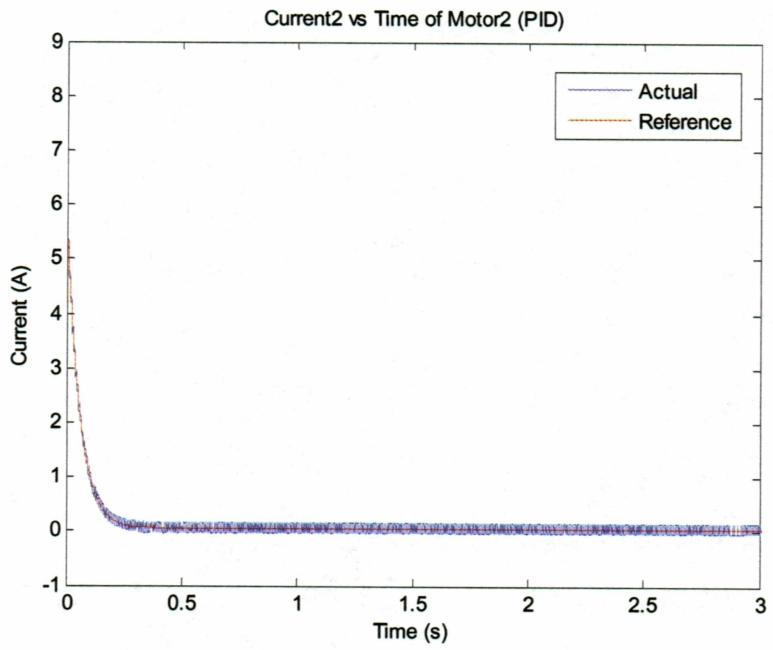

Fig. 4.16 Current variation of motor2.

4.6 Simulation Results of Geared System with PD+ Control

A unit step is applied as the reference to both joints and the simulations are conducted with $m_2 = 0.2\,\text{kg}$ and $m_2 = 0.4\,\text{kg}$, respectively. The gains obtained by the root locus analysis of PD control for $m_2 = 0.2\,\text{kg}$ are used in the simulations. Figs. 4.17 and 4.18 represent the variation of link angular position, Figs. 4.19 and 4.20 depict the variation of tracking errors, and the Fig. 4.21 shows the angular velocity of both the links. An important observation here is that link 1 and link 2 make steady-state errors of 0.007 and 0.003, respectively. This is again due to the load variation ($m_2 = 0.2\,\text{kg}$ to $m_2 = 0.4\,\text{kg}$) in the plant model and that the controller is unaware of this load variation.

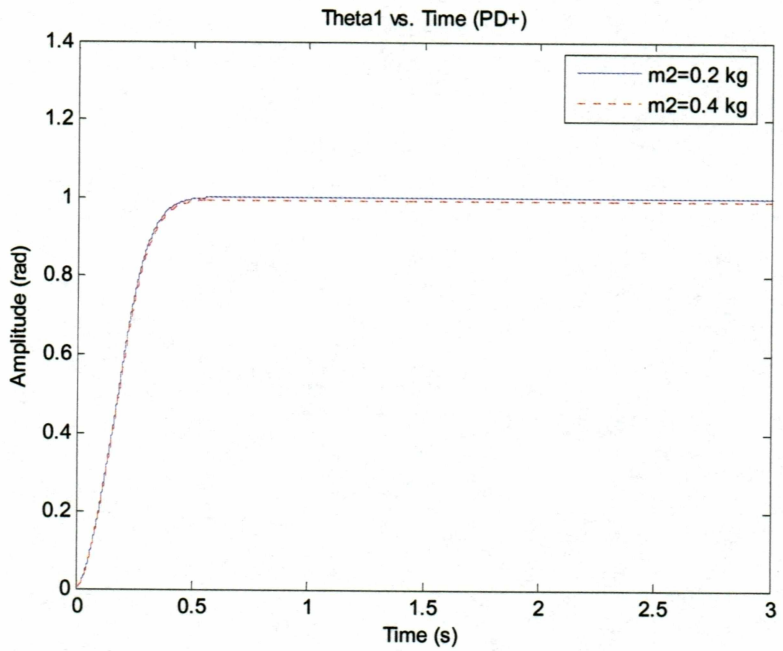

Fig. 4.17 Variation of angular position1 with change in the payload under PD+ control.

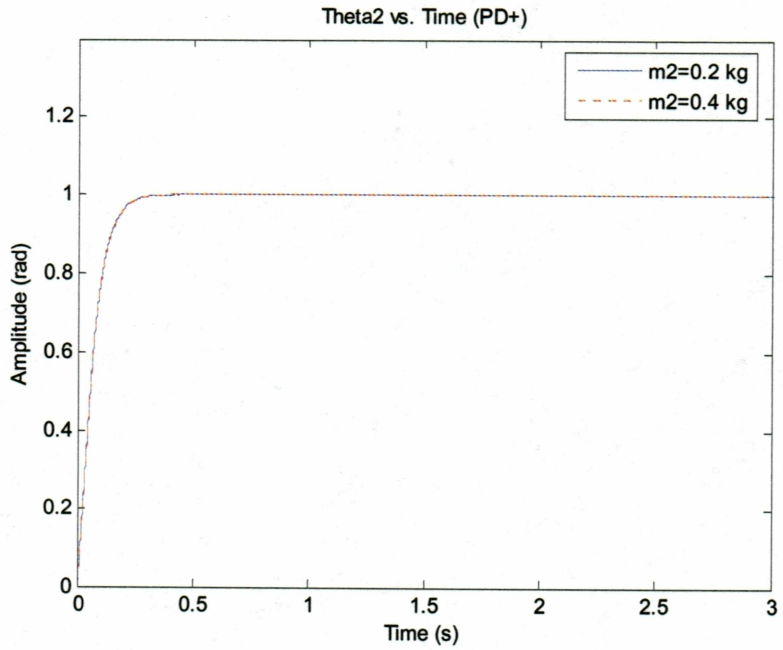

Fig. 4.18 Variation of angular position2 with change in the payload under PD+ control.

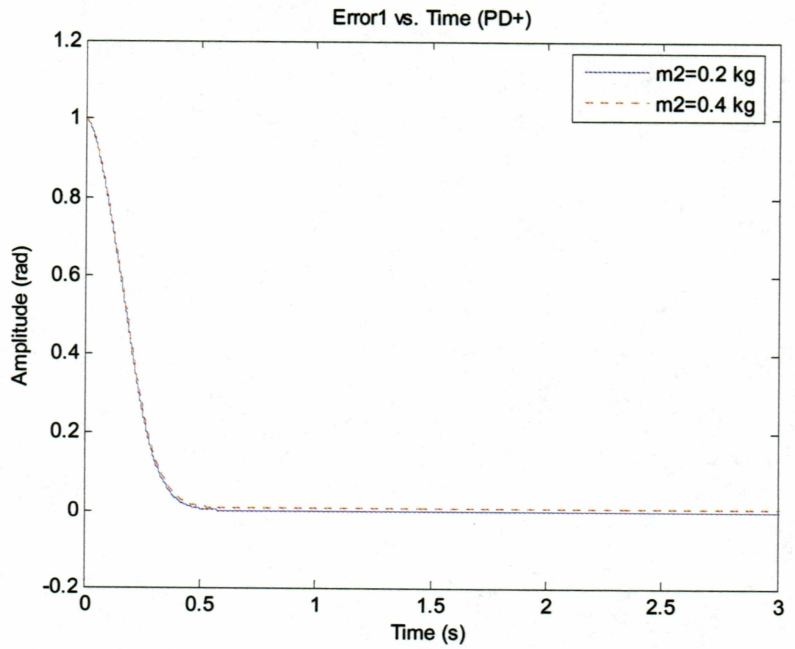

Fig. 4.19 Variation of tracking error1 with change in the payload under PD+ control.

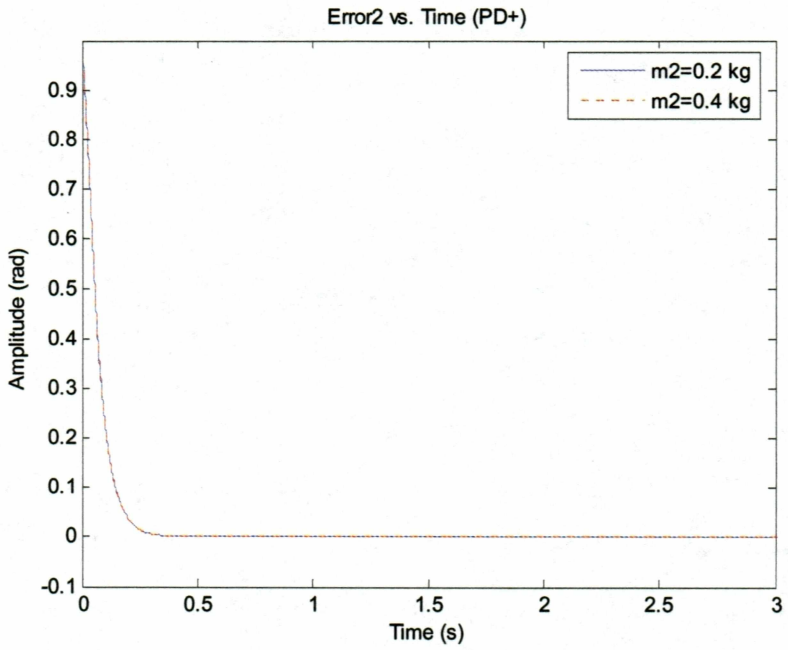

Fig. 4.20 Variation of tracking error2 with change in the payload under PD+ control.

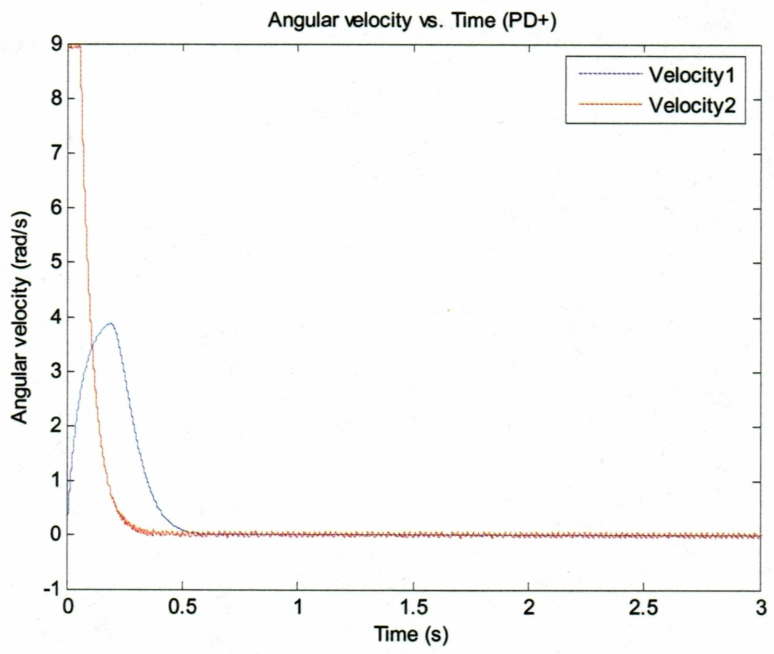

Fig. 4.21 Angular velocities of both motors under PD+ control.

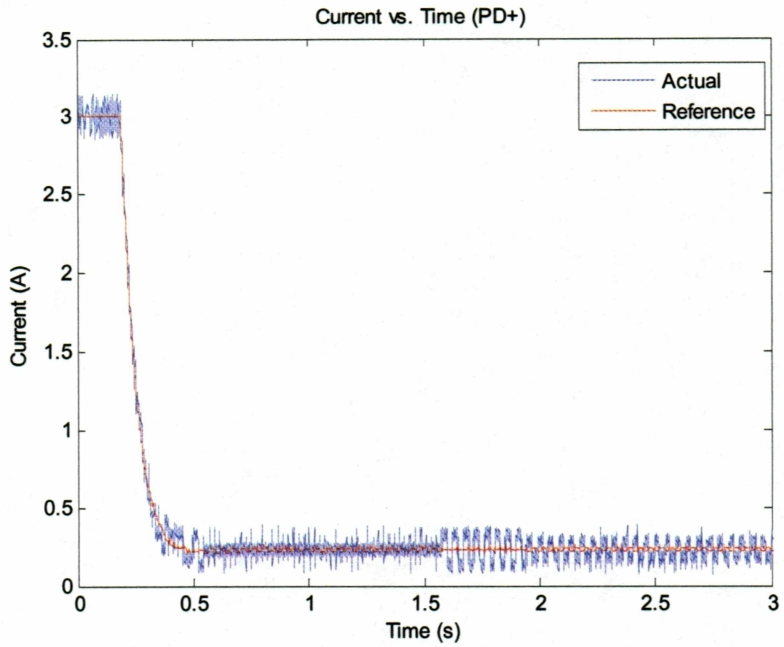

Fig. 4.22 Current variation of motor1.

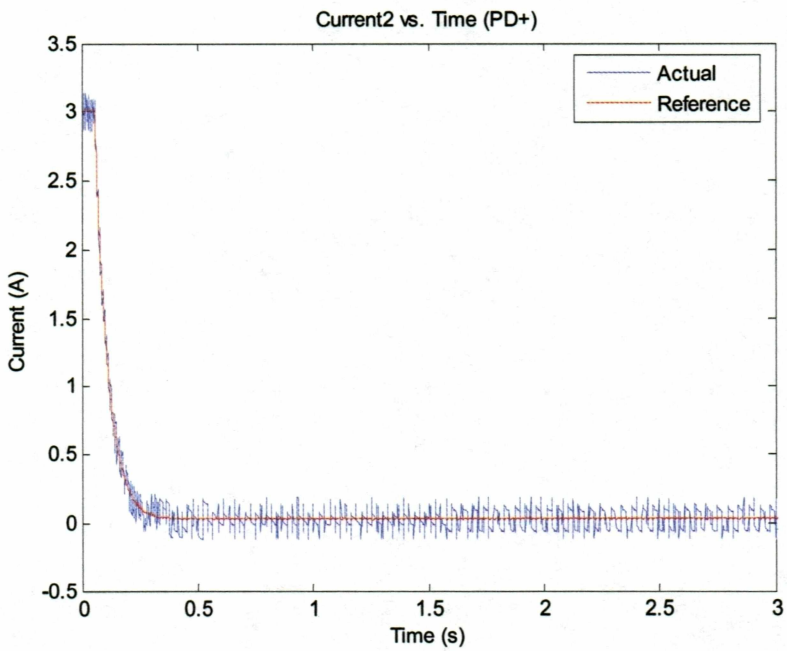

Fig. 4.23 Current variation of motor2.

Figs. 4.22 and 4.23 show the variation of current of the two motors. The currents consumed by the motors to hold the links of the robot at the desired positions are 24 mA and 4 mA.

4.7 Simulation Results of Geared System with SM Control

A unit step is applied as the reference to both joints and the simulations are conducted with $m_2 = 0.2\,\text{kg}$ and $m_2 = 0.4\,\text{kg}$. Figs. 4.24 and 4.25 represent the variation of angular positions, Figs. 4.26 and 4.27 depict the variation of tracking errors, and the Fig. 4.28 shows the angular velocity of both the motors. The SMC parameters for the desired error dynamics are chosen as $c_1 = 10$, $c_2 = 10$, $d_1 = 0.02$, and $d_2 = 0.02$.

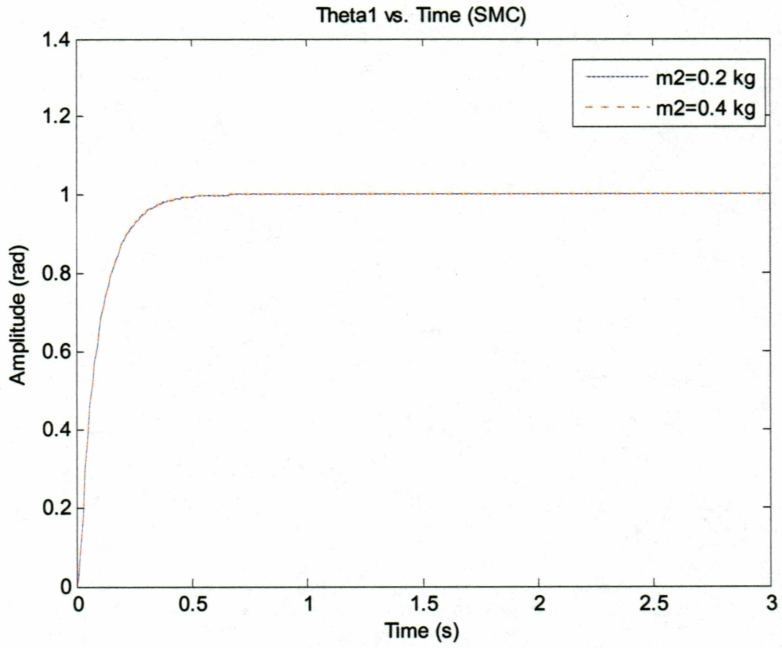

Fig.4.24 Variation of angular position1 with change in the payload under SM control.

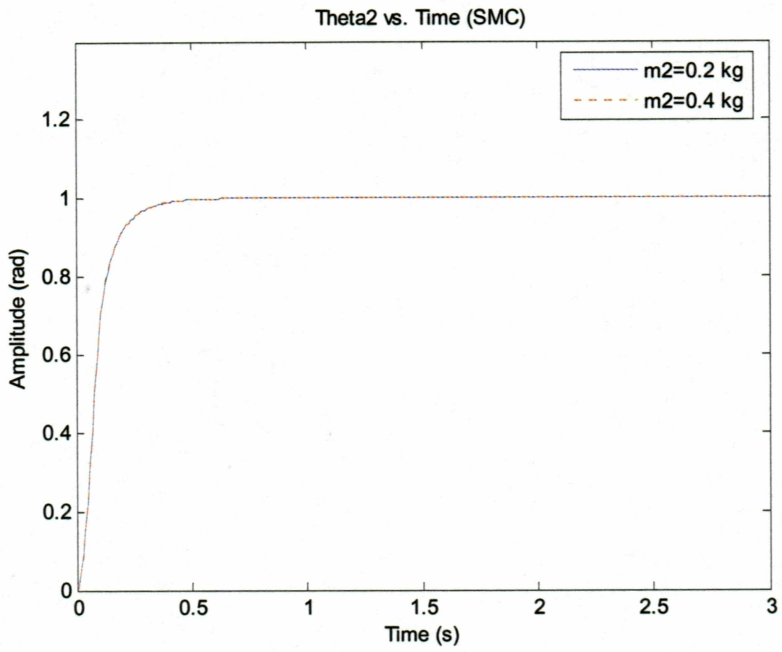

Fig. 4.25 Variation of angular position2 with change in the payload under SM control.

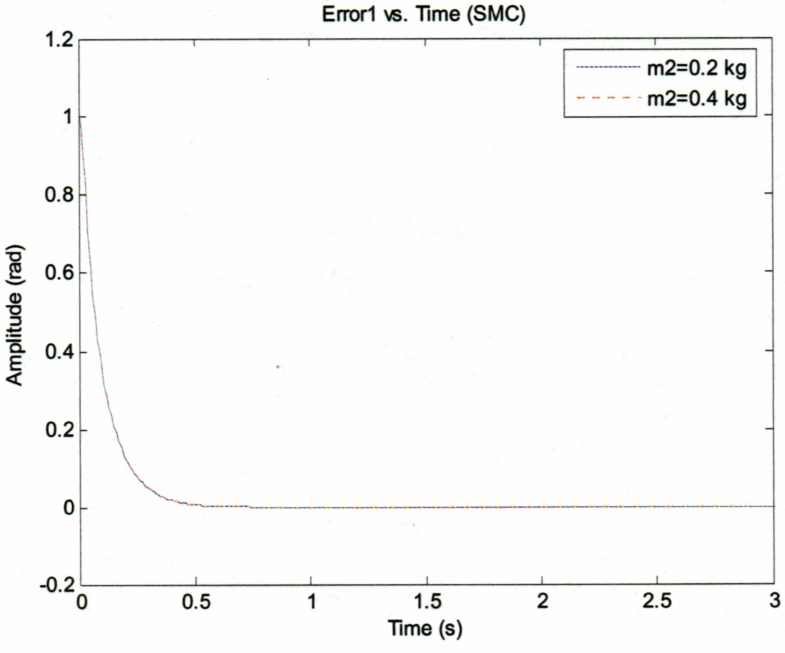

Fig. 4.26 Variation of tracking error1 with change in the payload under SM control.

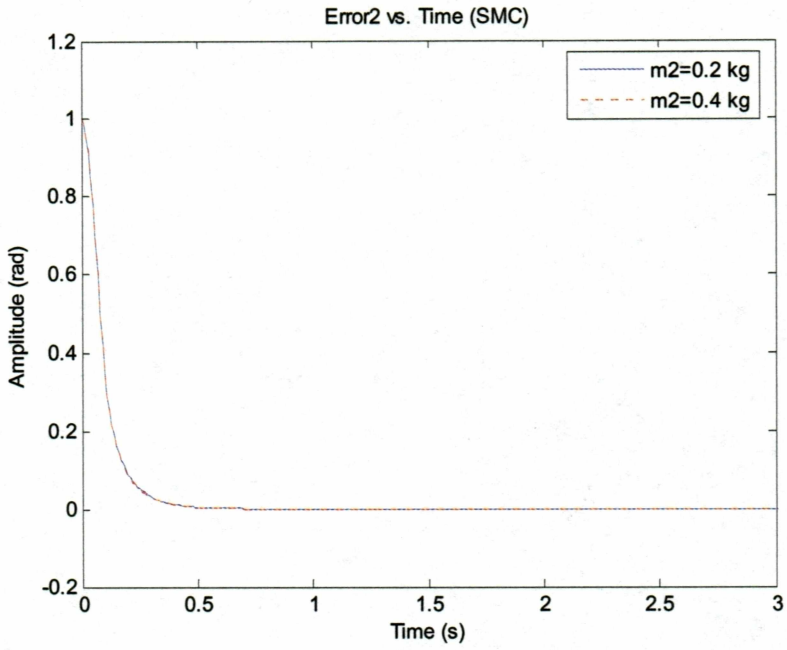

Fig. 4.27 Variation of tracking error2 with change in the payload under SM control.

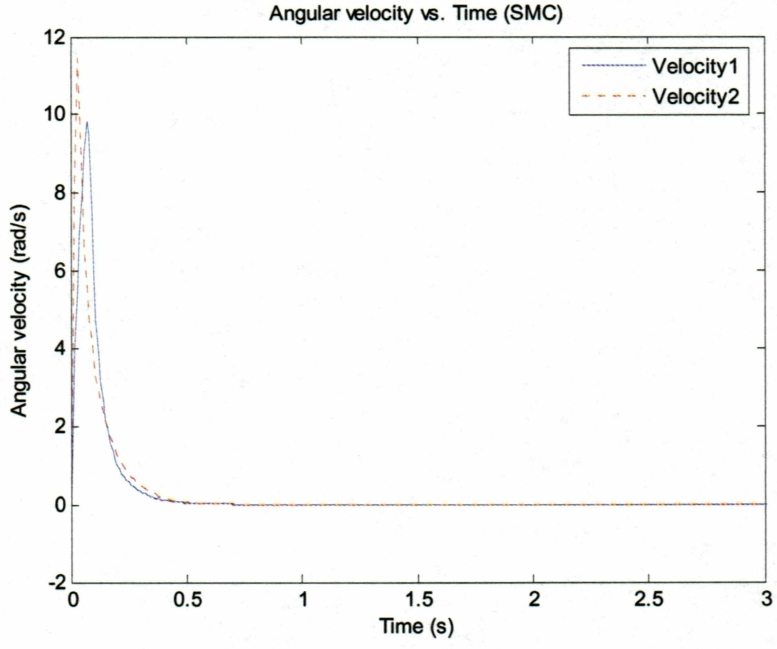

Fig. 4.28 Angular velocities of both motors under SM control.

Figs. 4.29 and 4.30 show the variation of current of the two motors. The currents consumed by the motors to hold the links at the desired positions are 24 mA and 4 mA. It is observed that there is no change in the performance of the SM controller in spite of the variation in the payload. Thus, the method has demonstrated the expected robustness to the load uncertainties. Fig. 4.33 shows the applied input voltage to the system.

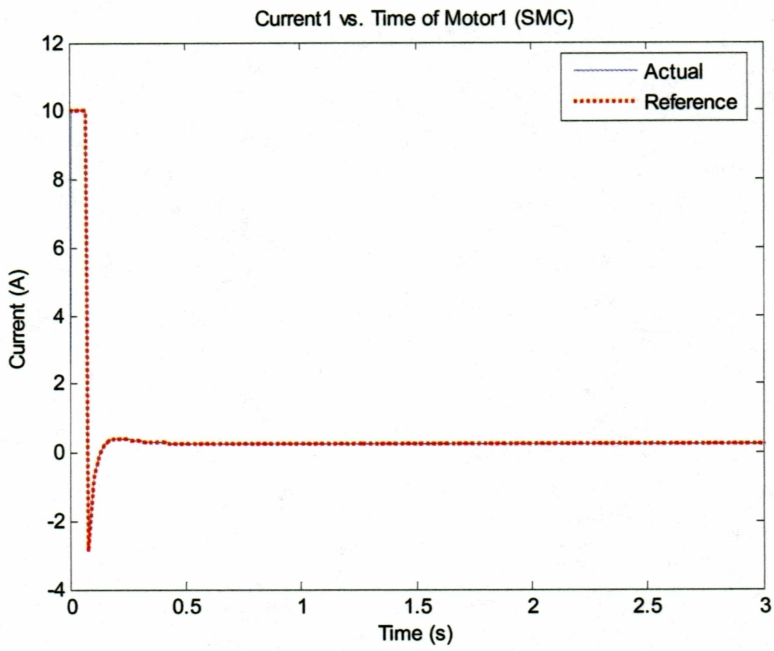

Fig. 4.29 Current variation of motor1.

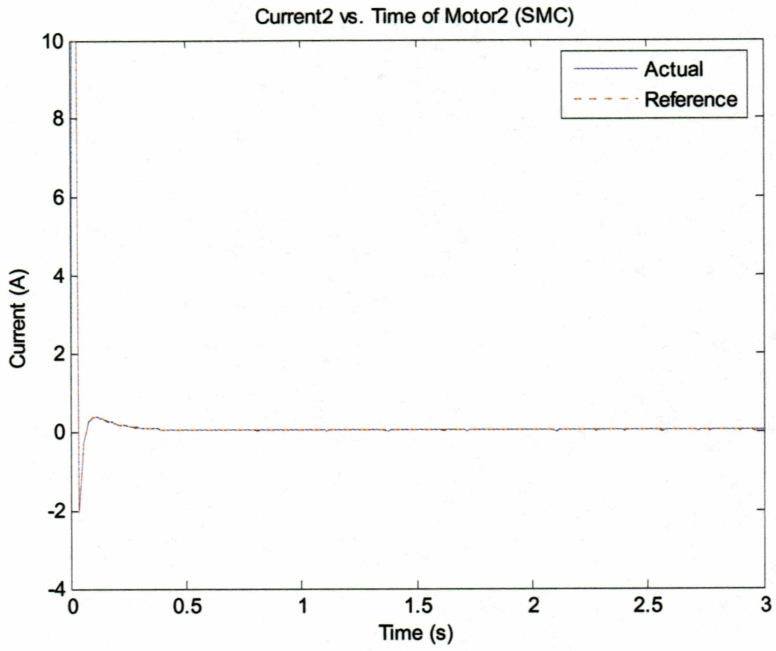

Fig. 4.30 Current variation of motor2.

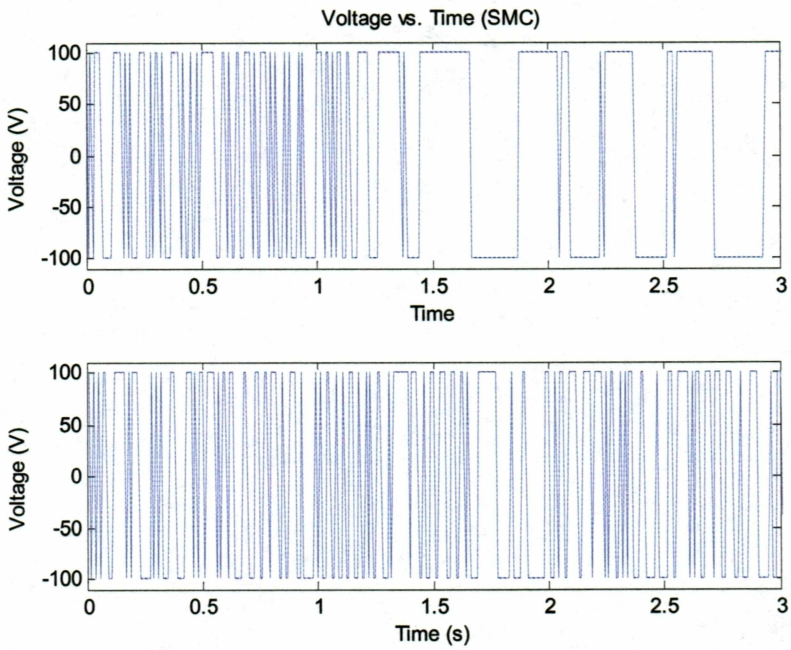

Fig. 4.31 Voltage variation of motors 1 and 2.

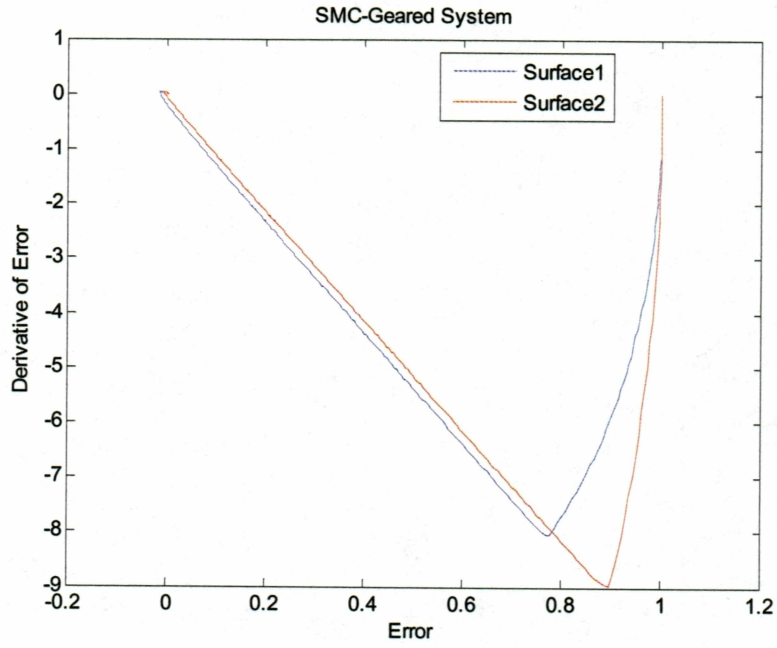

Fig. 4.32 Switching surface (Geared System) without load variation.

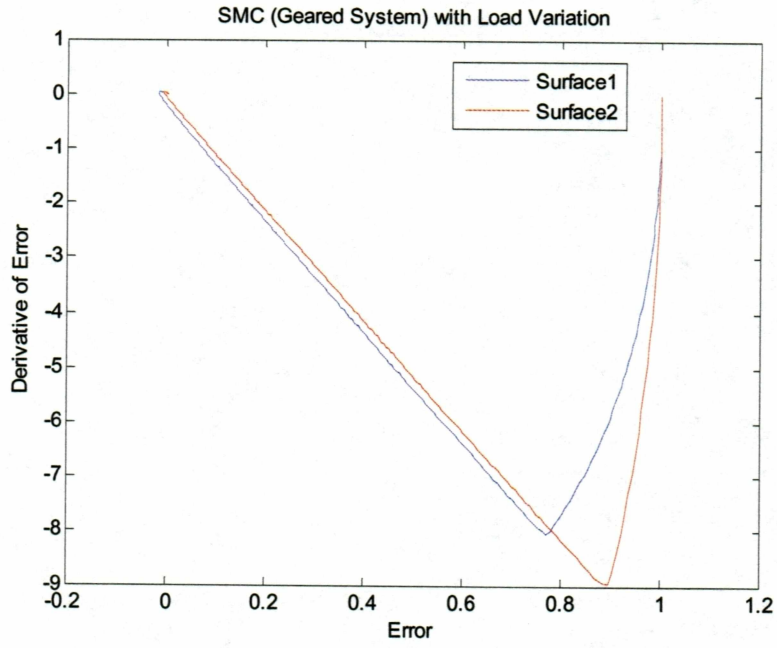

Fig. 4.33 Switching surface (Geared System) with load variation.

Figs. 4.32 and 4.33 demonstrate the phase portraits for the error dynamics. As can be seen in both situations (with and without load variation), once the error dynamics reaches the selected surface (representing the desired error dynamics), it stays on it until the error goes to zero. In other words, the complicated nonlinear system is forced to act like a 1st order linear system. The similarity of the error dynamics in both situations indicates the robustness of the control method.

4.8 Simulation Results of the Geared System for Sinusoidal Input

The same system is now subjected to a unit step reference for angular position1 and sinusoidal reference of amplitude one and frequency of 1/12 Hz for angular position2. The simulations are repeated for all four controllers under this condition. Fig. 4.34 shows the variation of angular positions 1&2 and Fig. 4.35 is the expanded version of Fig. 4.34 for a better demonstration of the system performance in steady-state with all controllers.

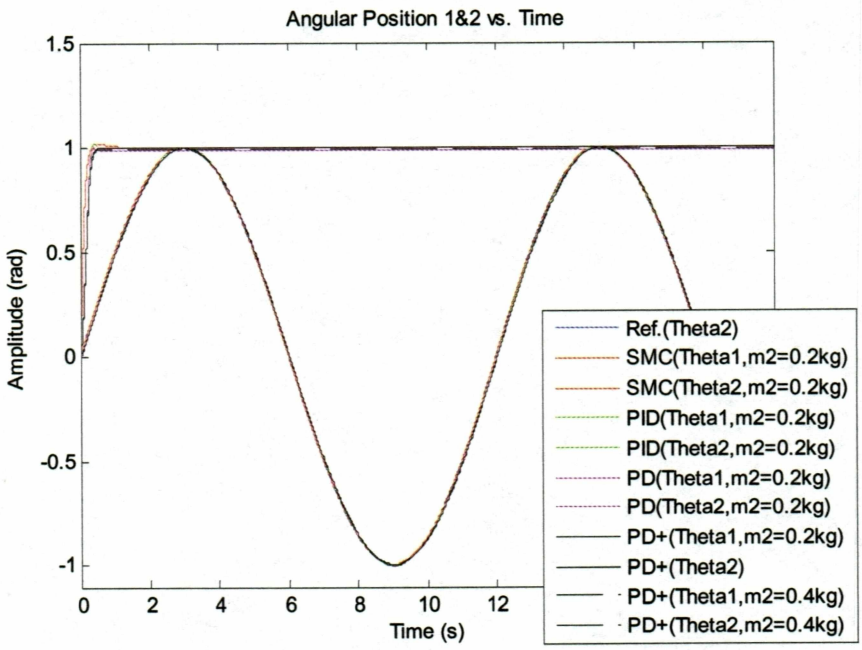

Fig. 4.34 Variation of angular positions 1&2 with different controllers.

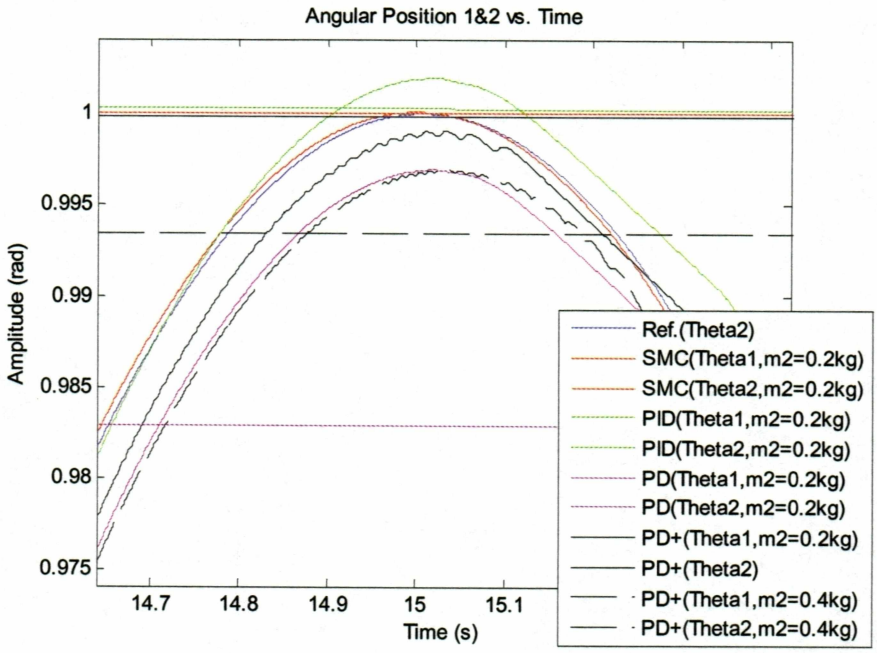

Fig. 4.35 Variation of angular positions 1&2 with different controllers.

The plot indicates that the PD controller results in the highest steady-state error, due to the disturbance present in the system. The PID control, on the other hand, has no steady-state error with the constant disturbance obtained with the step-type reference; however, it makes a steady-state error with the sinusoidal reference trajectory, as the disturbance is not constant anymore. As for the performance of the PD+ controller under accurate knowledge of the load, there is an almost negligible steady-state error due to the neglected nonlinearities of the PWM switching. However this error increases once a load variation has occurred. Finally, SMC is observed to demonstrate the best performance for both reference trajectories and in spite of load variation.

4.9 PD+ Control for Direct-Drive Systems

In this section, the PD+ controller and SMC will be evaluated for the more challenging control problem of a 2-DOF direct-drive robotic arm. The challenge is presented due to the removal of the gear mechanism. As a result, load variations and all the nonlinearities of the link dynamics are directly reflected to the actuators and vice versa, without the filtering effect of the gears. In this study, the model and parameters of an actual 2-DOF direct-drive arm are used. The motor used for both shoulder and elbow joints is the model DM1015-B from Parker Compumotor r, which is capable of delivering a torque of 15 Nm. The system parameters are

$m_1 = 23.902$ kg, $m_2 = 1.285$ kg

$l_1 = 0.45$ m, $l_2 = 0.45$ m

$l_{c1} = 0.091$ m, $l_{c2} = 0.083$

$g = 9.81\,\text{m/s}^2$

The motor1 parameters are:

$R_1 = 1$ Ohms, $L_1 = 0.01$ H

$K_{t1} = K_{b1} = 4.5$ Nm/A

Gear ratio $n_1 = 1$

$I_{m1} = 0.522\,\text{kg.m}^2$, $B_{m1} = 2.288$ Nm.s/rad

$I_1 = 1.266\,\text{kg.m}^2$, $I_2 = 0.093\,\text{kg.m}^2$

The motor2 parameters are:

$R_2 = 1$ Ohms, $L_2 = 0.01$ H

$K_{t2} = K_{b2} = 1.5$ Nm/A

Gear ratio $n_2 = 1$

$I_{m2} = 0.012\,\text{kg.m}^2$

$B_{m2} = 0.006$ Nm.s/rad

A unit step is applied as the reference to both joints and the simulations are conducted with $m_2 = 1.285\,\text{kg}$ and $m_2 = 2.57\,\text{kg}$. Figs. 4.36 and 4.37 represent the variation of angular positions, Figs. 4.38 and 4.39 depict the variation of tracking errors, and Fig. 4.40 demonstrates the angular velocity of both motors.

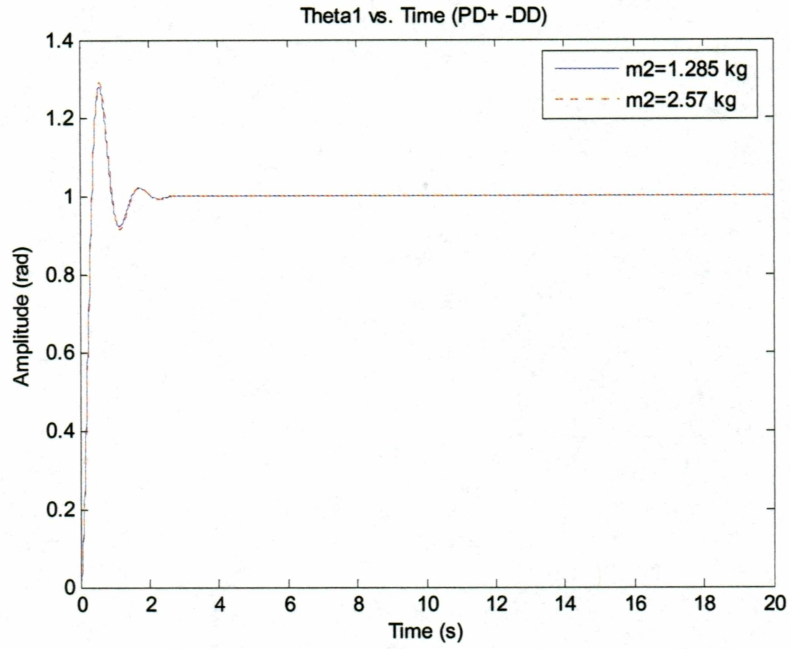

4.36 Variation of angular position1 with change in the payload under PD+ control.

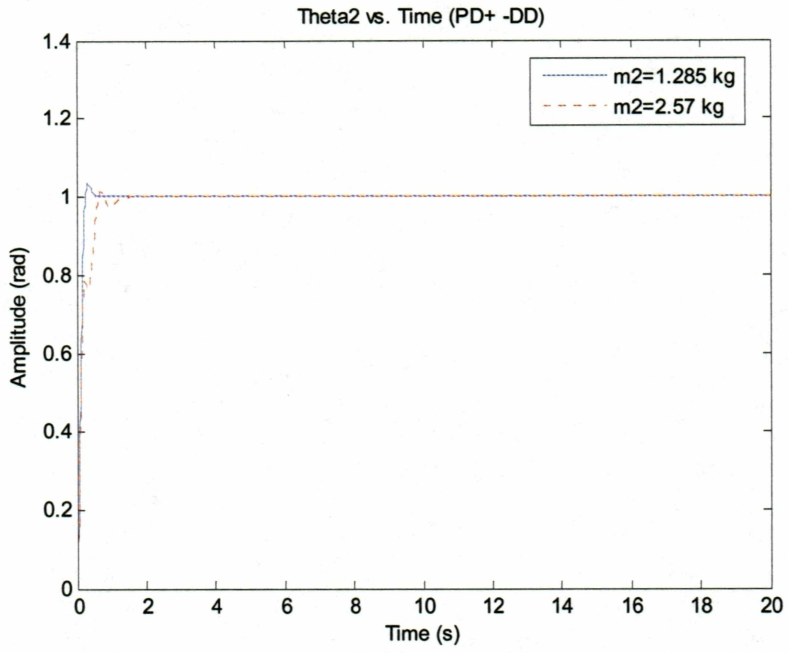

4.37 Variation of angular position2 with change in the payload under PD+ control.

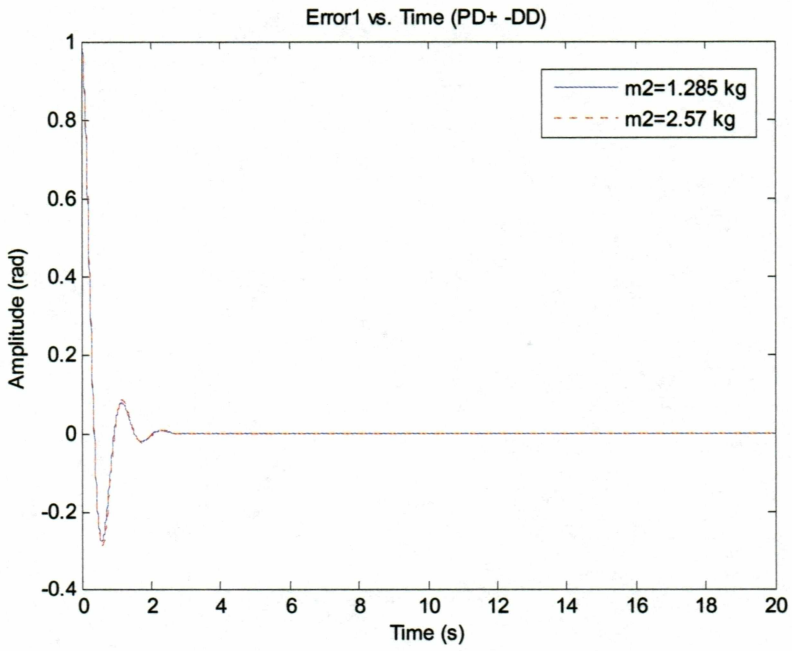

Fig. 4.38 Variation of tracking error1 with change in the payload under PD+ control.

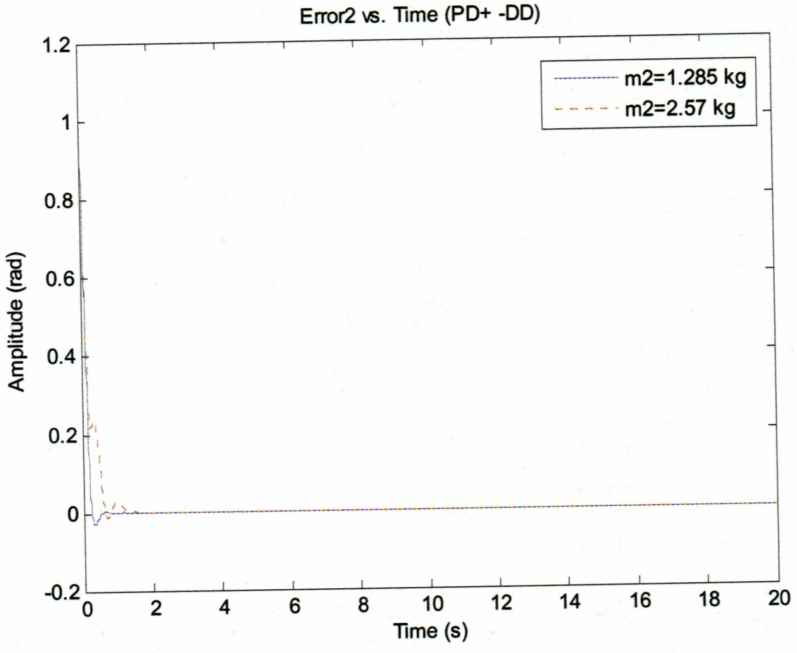

Fig. 4.39 Variation of tracking error2 with change in the payload under PD+ control.

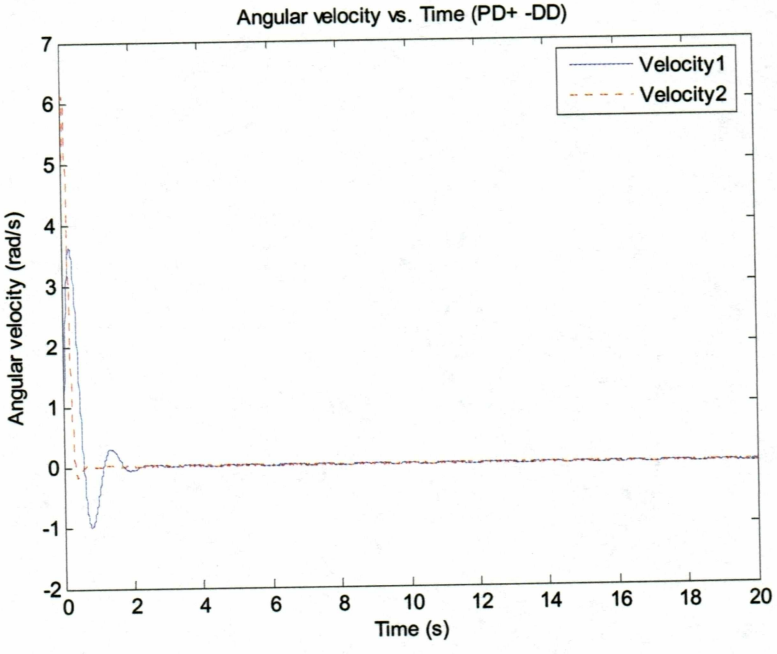

Fig. 4.40 Variation of angular position of motor 1 and 2.

The plots indicate a larger overshoot than desired with the PD design parameters. This is due to the augmented effect of nonlinearities as a result of the DD configuration.

4.10 SM Control for Direct-Drive System

Once again, a unit step is applied as the reference to both joints and the simulations are conducted with $m_2 = 1.285\,\text{kg}$ and $m_2 = 2.57\,\text{kg}$. Figs. 4.41 and 4.42 represent the variation of angular positions, Figs. 4.43 and 4.44 depict the variation of tracking errors, and Fig. 4.45 shows the angular velocity of both the links. The SMC parameters used for the desired error dynamics are $c_1 = 5$, $c_2 = 4$, $d_1 = 0.003$, and $d_2 = 0.003$.

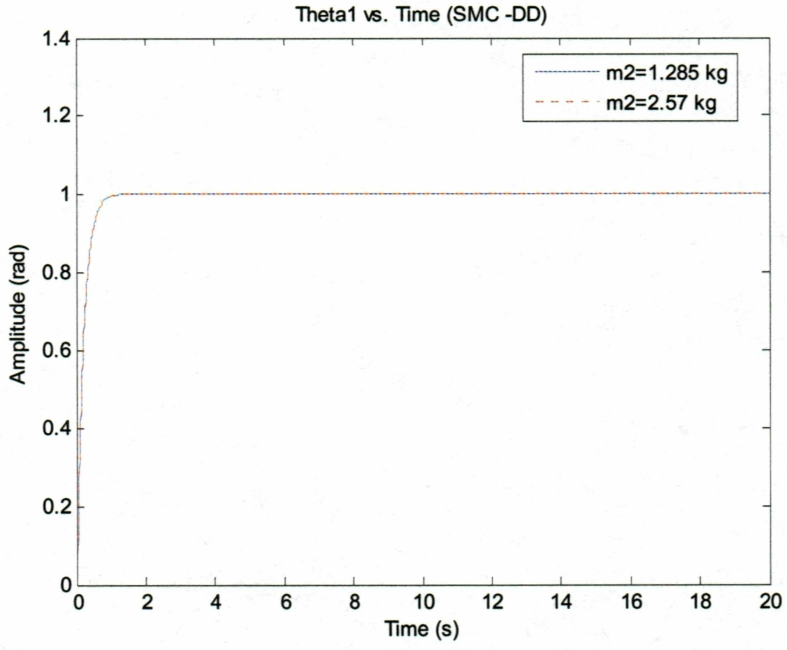

4.41 Variation of angular position1 with change in the payload under SM control.

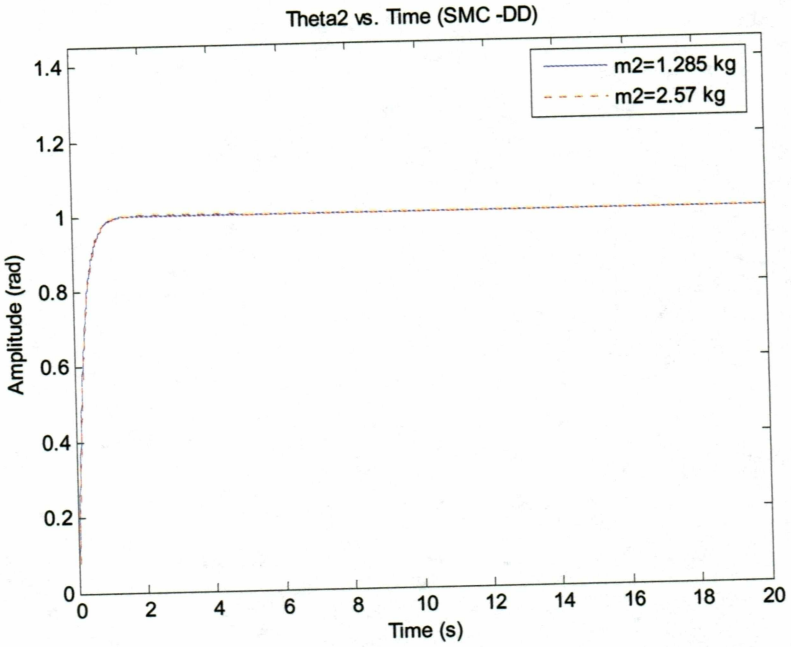

4.42 Variation of angular position2 with change in the payload under SM control.

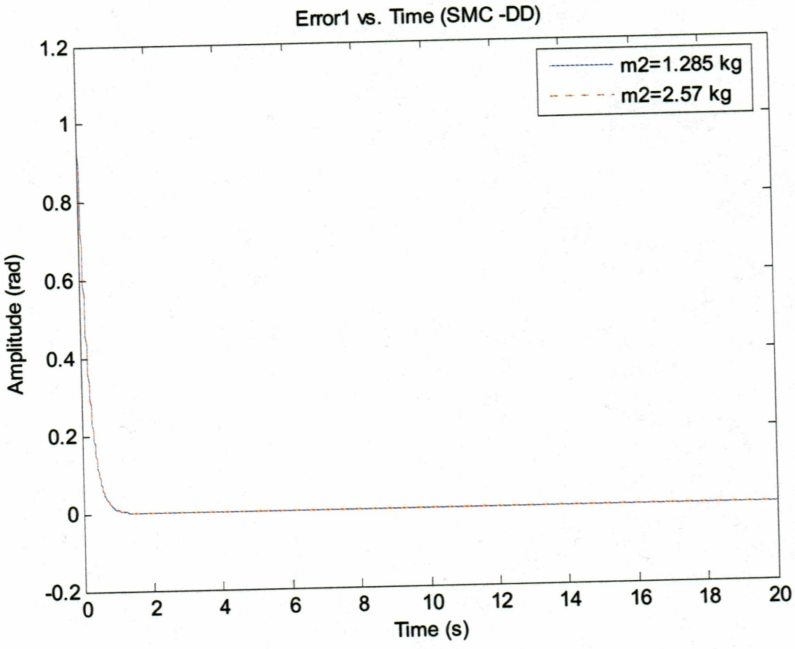

Fig. 4.43 Variation of tracking error1 with change in the payload under SM control.

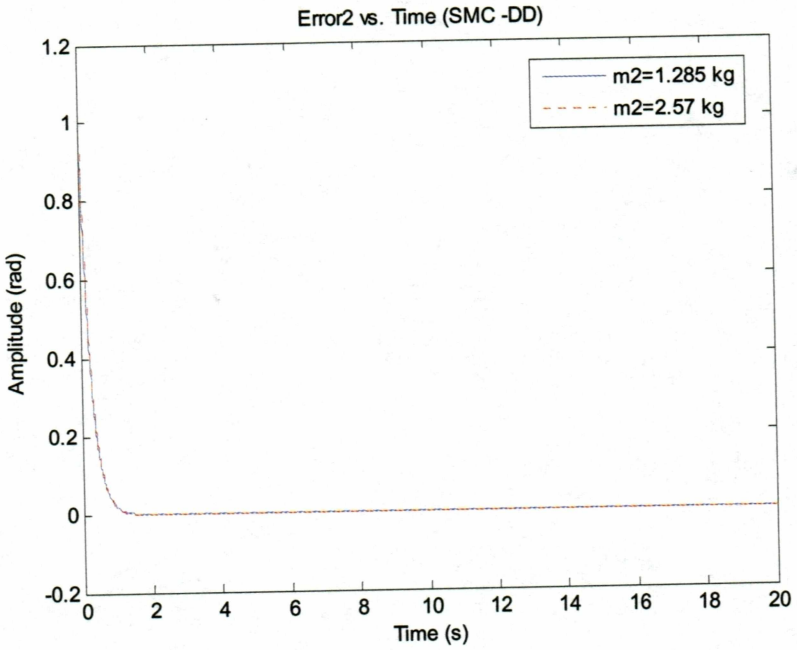

Fig. 4.44 Variation of tracking error2 with change in the payload under SM control.

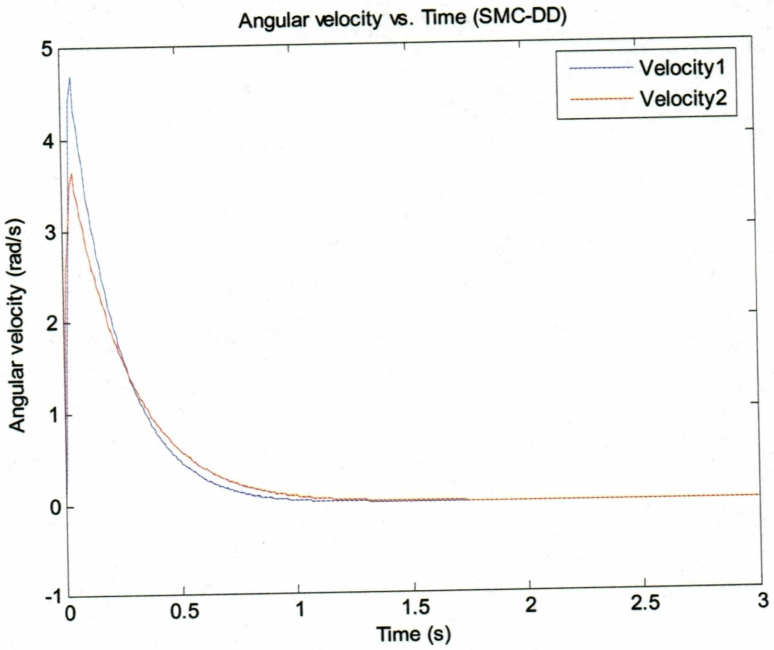

Fig. 4.45 Variation of angular velocity of motor 1 and 2.

Figs. 4.46 and 4.47 show the variation of current of the two motors. The currents consumed by the motors to hold the links at the desired positions are 3.39 A and 40 mA. Figs. 4.48 and 4.49 show the governing sliding surfaces for the direct-drive system. It is clear that the load variation does not cause any difference in system performance, indicating the robustness of SMC.

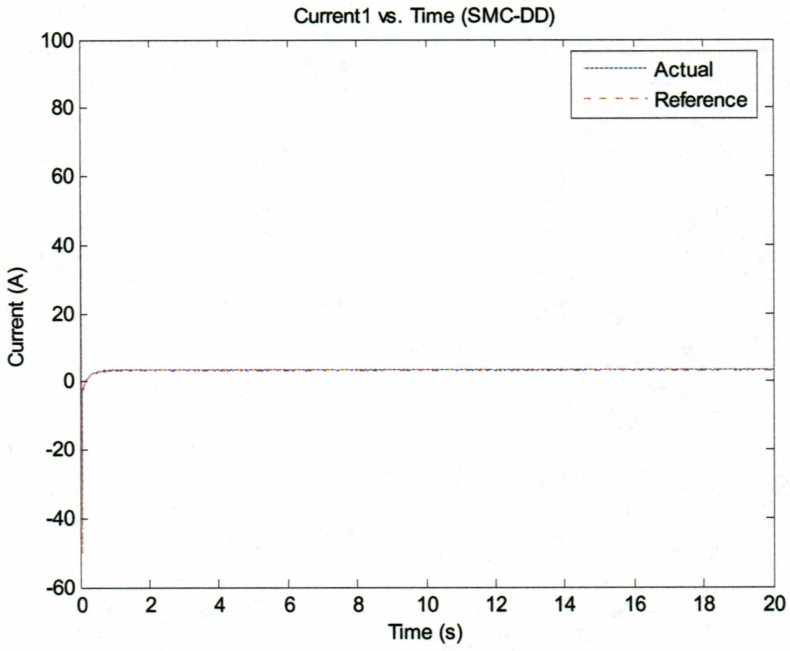

Fig. 4.46 Current variation of motor1.

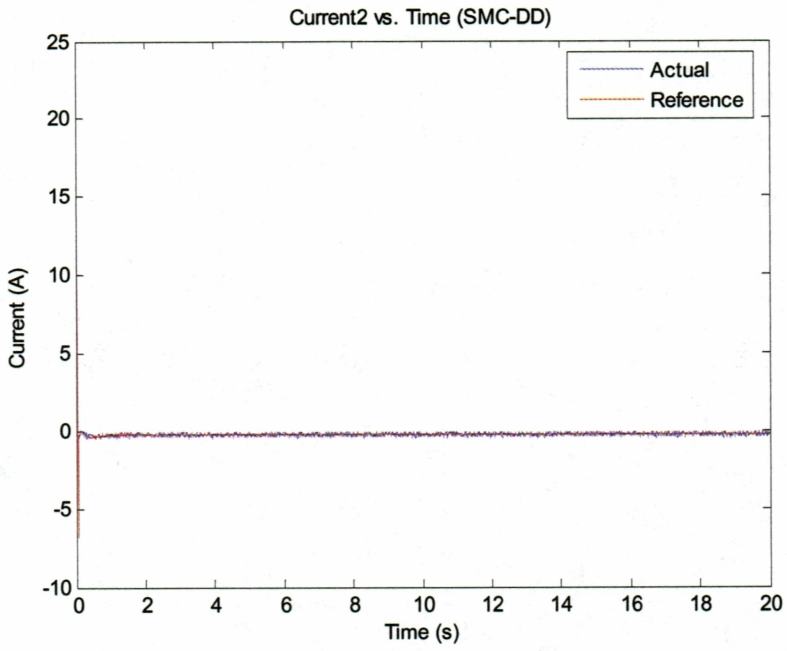

Fig. 4.47 Current variation of motor2.

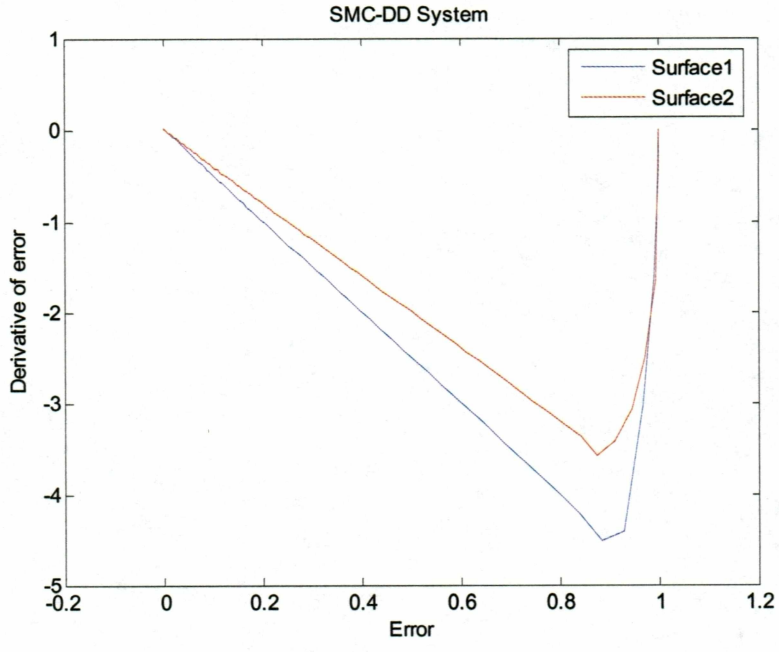

Fig. 4.48 Switching surface (DD System) without load variation.

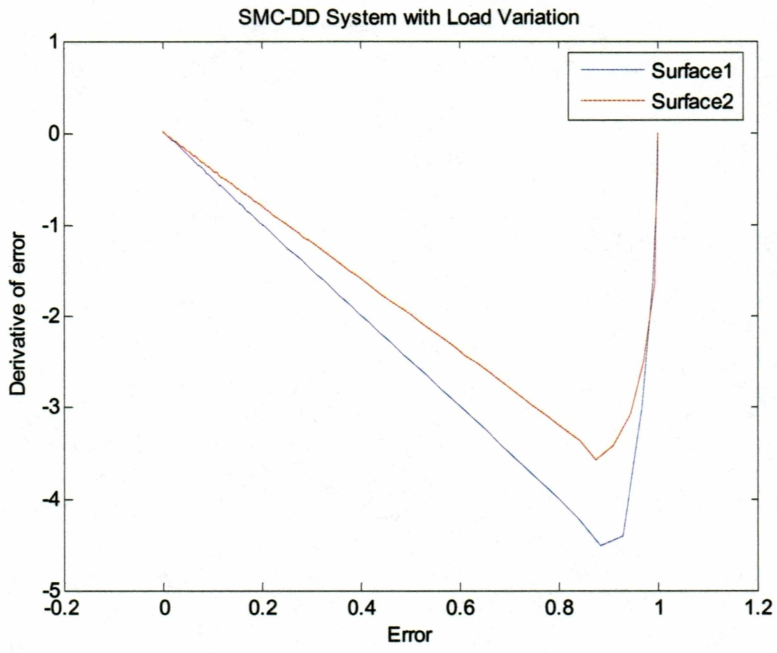

Fig. 4.49 Switching surface (DD System) with load variation.

4.11 Simulation Results of the Direct-Drive System for Sinusoidal Input

The same system is now subjected to a unit step reference for angular position1 and sinusoidal reference of amplitude one and frequency of 1/12 Hz for angular position2. The simulations are repeated for all four controllers under this condition. Fig. 4.50 shows the variation of angular positions 1&2, and Fig. 4.51 is the expanded version of Fig. 4.50 for a better demonstration of the system performance in steady-state with all controllers. Once again, the overshoot with step reference for the PD+ controller is caused by the removal of the gear mechanism in the DD system.

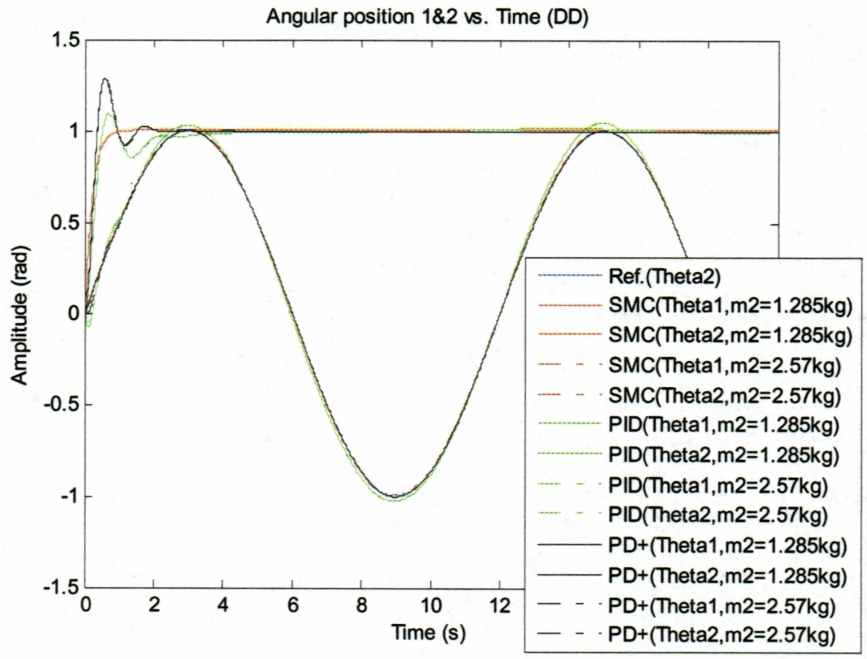

Fig. 4.50 Variation of angular positions 1&2 for link 1 (step) and link 2 (sinusoidal).

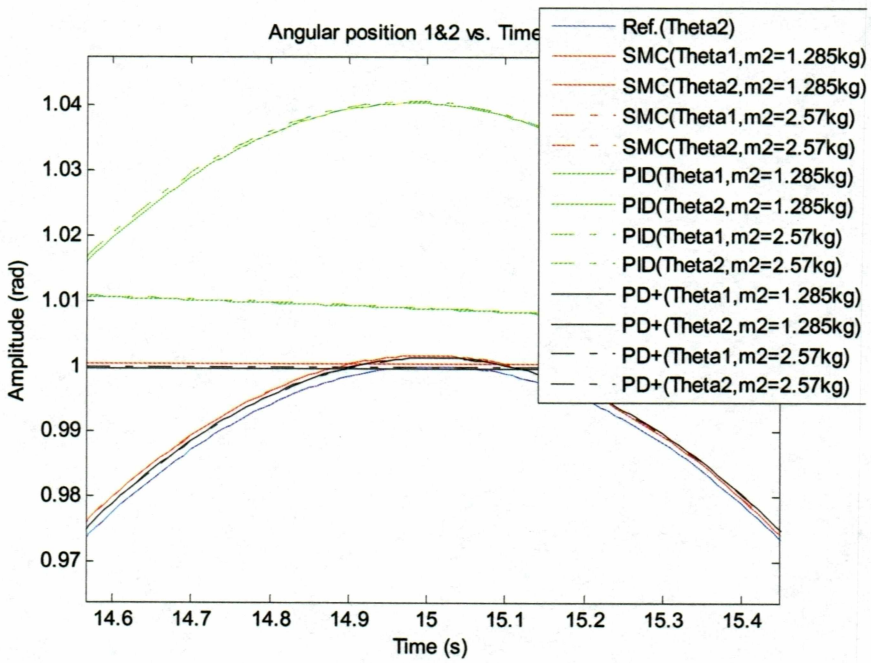

Fig. 4.51 Variation of angular positions 1&2 with different controllers.

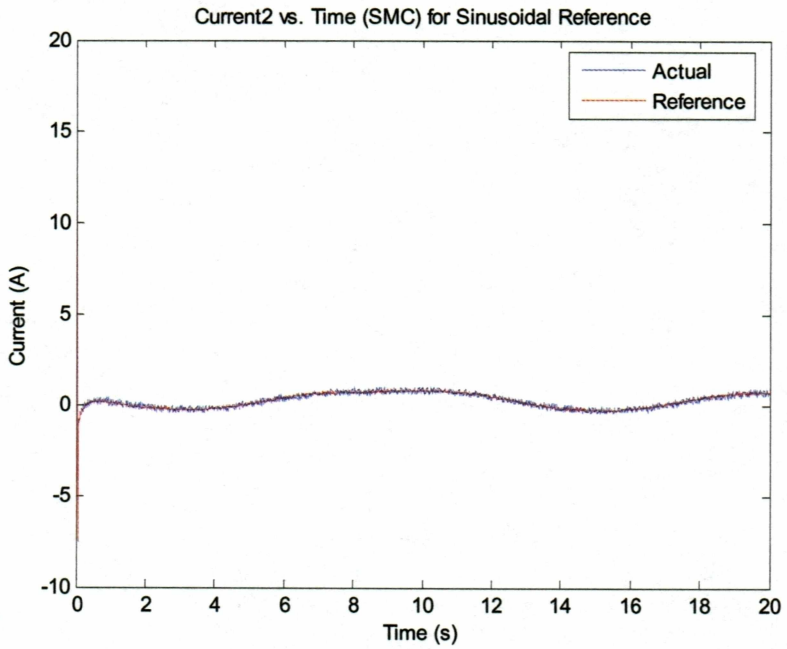

Fig. 4.52 Current variation of motor2.

4.12 Conclusions

The performance of various controllers is evaluated in this section for a 2 DOF geared and direct-drive planar elbow manipulator for both step and sinusoidal references. The PD controller, as expected, resulted in a steady state error. The PID controller served the purpose of reducing the steady state error significantly for step-type references but the response is slow. The PD+ is found to be more efficient in reducing the tracking errors if the plant model is known accurately. However, it resulted in the tracking errors both in transient and steady-state due to the uncertainties present in the model. The performance of sliding mode control of both geared and direct-drive systems is better than that of other controllers. It is clear that the performance of the SM control did not depend on the system model, and there is no change in the performance with variation in the load. Thus this controller exhibited robustness.

5. CONCLUSIONS AND FUTURE WORK

5.1 Conclusions

In this thesis work, a variety of control methods have been developed and evaluated on 2-DOF geared and direct-drive robotic manipulators under unknown load variations. The implemented control methods are linear PD and PID controllers, a model-based nonlinear PD+ controller and a chattering-free sliding mode controller (SMC), which is a novel application for both geared and direct-drive robotic arms subject to gravitational effects. The performance of the control methods has been tested for both step-type and sinusoidal reference joint trajectories. The following conclusions are drawn as a result of the evaluations;

- Due to the gravitational effects, which are effective in the given planar configuration, the PD controller has resulted in a constant steady-state error, even with step-type joint references. This error has increased with load variations, which are not taken into account in the root locus based design of PD parameters. Similarly, sinusoidal inputs have increased the error even more both in transient and steady-state.
- The PID controller, which is obtained from the PD controller with the addition of an integral term, is designed with the same PD parameters as in the previous step. As expected, this controller has yielded zero steady-state error for step-type joint reference, due to the constant gravitational effects the step function causes. However, with sinusoidal joint trajectories, the steady-state error is no longer zero, as gravitational effects are no longer constant, either.
- The PD+ controller ideally offers the best performance in transient and steady-state, provided the full system dynamics and load variations are known in advance and compensated accurately. This situation has been demonstrated in the good performance obtained with the exact compensation of system dynamics and load. However, with the unknown variation of load, errors have increased both in transient and steady-state. Another point worth noting is the

slight steady-state error obtained even with the "exact" compensation of dynamics. This is due to the fact that the PD+ does not compensate for the actuator dynamics arising from the PWM generation. However, this nonlinear effect has been taken into account as a hysteresis function in the simulation model to provide a realistic representation of the actual system.

- The results indicate that the PD+ controller should be combined with an on-line parameter estimation scheme to increase accuracy and robustness.
- Considering requirements and outcomes of the above mentioned controllers, the chattering-free SMC has been the most effective, as it has provided increased accuracy and robustness under unknown gravitational loads. An important attraction of SMC is that it requires no a priori knowledge of the system model and parameters and will keep the error dynamics on the selected sliding surface once it is reached.
- Additionally, it has been seen that the control of the direct-drive system is more challenging than control of gear systems, due to the increased effect of nonlinearities and uncertainties. Therefore, the control of direct-drive robotic systems definitely requires sophisticated controllers, such as linearization methods combined with online parameter estimation, or robust control approaches, such as SMC. Classical controllers cannot meet the performance requirements of direct-drive systems.

5.2 Future Work

- The study of the 2-DOF direct-drive arm should be continued with the consideration of space harmonic based torque ripple in the system dynamics. The effect of current dynamics has already been included in this thesis. However, torque harmonics of the actuator also have a significant effect on the performance of direct-drive manipulators. This issue is well known, but has not yet been studied in the depth it deserves in the current literature.

References

H. Berghuis, H. Roebbers, H. Nijmeijer, "Experimental comparison of parameter estimation methods in adaptive control", Automatica, 1995, 31(9), pp. 1275-1285.

S. O. Bogosyan, M. Gokasan, "Adaptive torque ripple minimization of permanent magnet synchronous motors for direct drive applications", Proceedings of IEEE IAS Annual Meeting, Vol. 1, Orlando, FL, Oct. 1995, pp. 231-237.

S. O. Bogosyan, Robot Control, lecture notes, 2004.

H.T. Chen, P. Jiang, W.H. Zhu, Y.J. Wang, "Comparative study of D.D. robot control algorithms for trajectory tracking", 12th IFAC World Congress, Sydney, Australia, Vol. 6, July 1993, pp.157-160.

B. De Jager, J. Banens, "Experimental evaluation of robot controllers", Proceedings of the 33rd Conference on Decision and Control, Dec.1994, Lake Buena Vista, FL, USA, pp. 363-368.

K. Erbatur, M.O. Kaynak, A. Sabanovic, "A study on robustness property of sliding-mode controllers: a novel design and experimental investigations", Industrial Electronics, IEEE Transactions, Vol. 46, Issue 5, Oct. 1999, pp. 1012 – 1018.

A. Jaritz, M. W. Spong, "An experimental comparison of robust control algorithms on a direct drive manipulator", IEEE Transactions on Control System Technology, 1996, Vol. 4, pp. 627-640.

John J. Craig, "Introduction to Robotics: Mechanics and Control", Prentice Hall, NJ, 1989.

K. Kim, Y. Hori, "Experimental evaluation of adaptive and robust schemes for robot manipulator control", IEEE Transactions on Industrial Electronics, 1995, 42(6), pp. 653-662.

T. Kokkinis, R. Stoughton, "Dynamics and control of closed-chain robot arms with application to a new direct-drive robot arm", IASTED International Journal of Robotics and Automation, 1991, 6(1), pp. 25-34.

F. Lewis, M. W. Spong, C. Abdallah, "Robot Control: Dynamics, Motion Planning, and Analysis", IEEE Press, 1992.

G. Liu, AA. Goldenberg, "Comparative study of robust saturation-based control of robot manipulators: analysis and experiments", The International Journal of Robotics Research, 1996, 15(5), pp. 473-491.

Z. Lu, KB. Shimoga, AA. Goldenberg, "Experimental determination of dynamic parameters of robot arms", Journal of Robotic Systems, 1993, 10(8), pp.1009-1029.

Mark W. Spong, M. Vidyasagar, "Robot Dynamics and Control", John Wiley & Sons, Inc., Canada, 1989.

M.W. Spong, "On the robust control of robot manipulators", IEEE Transactions on Automatic Control, 1992, 37(11), pp. 1782-1786.

F. Reyes, R. Kelly, "Experimental evaluation of model-based controllers on a direct drive robot arm", Mechatronics, 11, 2001, pp. 267-282.

V. Santibanez, R. Kelly, F. Reyes, "A new set-point controller with bounded torques for robot manipulators", IEEE Transactions on Industrial Electronics, Vol. 45, no.1, 1998, pp. 126-133.

E. Slotine, W. Li, "Applied Nonlinear Control", Prentice Hall, NJ, 1991.

L.L. Whitcomb, A.A. Rizzi, D.E. Koditschek, "Comparative experiments with a new adaptive controller for robot arms", IEEE Transactions on Robotics and Automation, 1993, 9(1), pp. 59-70.

Z. Yu, H. Chen and P. Woo, "Polytopic gain scheduled H_∞ control for robotic manipulators", Robotica, Vol.21, pp. 495-504, 2003.

APPENDIX

Euler-Lagrange Formulation for Planar Elbow Manipulator:

The position vectors of both masses m_1 and m_2 are given by

$$r_1 = l_1 \cos\theta_1 \; i + l_1 \sin\theta_1 \; j$$

$$r_2 = (l_1 \cos\theta_1 + l_2 \cos(\theta_1 + \theta_2))i + (l_1 \sin\theta_1 + l_2 \sin(\theta_1 + \theta_2))\, j$$

The respective velocities are given by

$$V_1 = \dot{r}_1 = -l_1 \sin\theta_1 \, \dot{\theta}_1 \, i + l_1 \cos\theta_1 \, \dot{\theta}_1 \, j$$

$$V_2 = \dot{r}_2 = (-l_1 \sin\theta_1 \, \dot{\theta}_1 - l_2 \sin(\theta_1 + \theta_2)(\dot{\theta}_1 + \dot{\theta}_2))i + (l_1 \cos\theta_1 \, \dot{\theta}_1 + l_2 \cos(\theta_1 + \theta_2)(\dot{\theta}_1 + \dot{\theta}_2))\, j$$

The kinetic energy of the system can be derived as

$$V_1^2 = \dot{r}_1 \dot{r}_1 = l_1^2 \dot{\theta}_1^2$$

$$V_2^2 = \dot{r}_2 \dot{r}_2 = l_1^2 \dot{\theta}_1^2 + l_2^2 (\dot{\theta}_1 + \dot{\theta}_2)^2 + 2 l_1 l_2 (\dot{\theta}_1^2 + \dot{\theta}_1 \dot{\theta}_2) \cos\theta_2$$

$$k_1 = \frac{1}{2} m_1 l_1^2 \dot{\theta}_1^2$$

$$k_2 = \frac{1}{2} m_2 (l_1^2 \dot{\theta}_1^2 + l_2^2 (\dot{\theta}_1 + \dot{\theta}_2)^2 + 2 l_1 l_2 (\dot{\theta}_1^2 + \dot{\theta}_1 \dot{\theta}_2) \cos\theta_2)$$

$$k = k_1 + k_2 = \frac{1}{2} l_1^2 \dot{\theta}_1^2 (m_1 + m_2) + \frac{1}{2} m_2 l_2^2 (\dot{\theta}_1 + \dot{\theta}_2)^2 + l_1 l_2 (\dot{\theta}_1^2 + \dot{\theta}_1 \dot{\theta}_2) \cos\theta_2$$

The potential energy is then calculated.

$$u_1 = m_1 g l_1 \sin\theta_1$$

$$u_2 = m_2 g (l_1 \sin\theta_1 + l_2 \sin(\theta_1 + \theta_2))$$

$$u = u_1 + u_2 = m_1 g l_1 \sin\theta_1 + m_2 g (l_1 \sin\theta_1 + l_2 \sin(\theta_1 + \theta_2))$$

Using the Lagrangian formulation

$$\frac{d}{dt}\frac{\partial L}{\partial \dot{\Theta}} - \frac{\partial L}{\partial \Theta} = \tau$$

We have

$$L = k - u = \frac{1}{2}(l_1^2\dot{\theta}_1^2(m_1+m_2) + m_2 l_2^2(\dot{\theta}_1+\dot{\theta}_2)^2) + m_2 l_1 l_2(\dot{\theta}_1^2 + \dot{\theta}_1\dot{\theta}_2)\cos\theta_2 - m_1 g l_1 \sin\theta_1 - m_2 g(l_1\sin\theta_1 + l_2\sin(\theta_1+\theta_2)$$

$$\frac{\partial L}{\partial \dot{\theta}_1} = (m_1+m_2)l_1^2\dot{\theta}_1 + m_2 l_2^2(\dot{\theta}_1+\dot{\theta}_2) + m_2 l_1 l_2(2\dot{\theta}_1+\dot{\theta}_2)\cos\theta_2$$

$$\frac{d}{dt}\frac{\partial L}{\partial \dot{\theta}_1} = (m_1+m_2)l_1^2\ddot{\theta}_1 + m_2 l_2^2(\ddot{\theta}_1+\ddot{\theta}_2) + m_2 l_1 l_2(2\ddot{\theta}_1+\ddot{\theta}_2)\cos\theta_2 - m_2 l_1 l_2(2\dot{\theta}_1+\dot{\theta}_2)\sin\theta_2\dot{\theta}_2$$

$$\frac{\partial L}{\partial \theta_1} = -(m_1+m_2)gl_1\cos\theta_1 - m_2 g l_2(\theta_1+\theta_2)$$

Substituting the above two equations in the Lagrangian, we have

$$\tau_1 = m_2 l_2^2(\ddot{\theta}_1+\ddot{\theta}_2) + (m_1+m_2)l_1^2\ddot{\theta}_1 + m_2 l_1 l_2 c_2(2\ddot{\theta}_1+\ddot{\theta}_2) - m_2 l_1 l_2 s_2\dot{\theta}_2^2 - 2m_2 l_1 l_2 s_2\dot{\theta}_1\dot{\theta}_2 + m_2 l_2 g c_{12} + (m_1+m_2)l_1 g c_1$$

where $c_1 = \cos\theta_1$
$c_2 = \cos\theta_2$
$s_2 = \sin\theta_2$
$c_{12} = \cos(\theta_1+\theta_2)$

The above same process is carried out for θ_2 and we can have the second equation of motion as

$$\tau_2 = m_2 l_2^2(\ddot{\theta}_1+\ddot{\theta}_2) + m_2 l_1 l_2 c_2\ddot{\theta}_1 + m_2 l_2 s_2\dot{\theta}_1^2 + m_2 l_2 g c_{12}$$

Converting Equations of Motion into State-space:

The equations of motion are given by (including their respective motor inertia and friction terms)

$$\tau_1 = I_{m1}\ddot{\theta}_1 + B_{m1}\dot{\theta}_1 + m_2 l_2^2(\ddot{\theta}_1 + \ddot{\theta}_2) + (m_1 + m_2)l_1^2\ddot{\theta}_1 + m_2 l_1 l_2 c_2(2\ddot{\theta}_1 + \ddot{\theta}_2) - m_2 l_1 l_2 s_2 \dot{\theta}_2^2 - 2m_2 l_1 l_2 s_2 \dot{\theta}_1\dot{\theta}_2 + m_2 l_2 g c_{12} + (m_1 + m_2)l_1 g c_1$$

$$\tau_2 = I_{m2}\ddot{\theta}_2 + B_{m2}\dot{\theta}_2 + m_2 l_2^2(\ddot{\theta}_1 + \ddot{\theta}_2) + m_2 l_1 l_2 c_2 \ddot{\theta}_1 + m_2 l_2 s_2 \dot{\theta}_1^2 + m_2 l_2 g c_{12}$$

taking out the linear coefficients of $\ddot{\theta}$, we have

$$\ddot{\theta}_1 = \frac{1}{m_2 l_2^2 + (m_1 + m_2)l_1^2 + I_{m1}}(-w_1 + \tau_1 - B_{m1}\dot{\theta}_1)$$

$$\ddot{\theta}_2 = \frac{1}{m_2 l_2^2 + I_{m2}}(-w_2 + \tau_2 - B_{m2}\dot{\theta}_2)$$

where

$$w_1 = m_2 l_2^2 \ddot{\theta}_2 + m_2 l_1 l_2 c_2(2\ddot{\theta}_1 + \ddot{\theta}_2) - m_2 l_1 l_2 s_2 \dot{\theta}_2^2 - 2m_2 l_1 l_2 s_2 \dot{\theta}_1\dot{\theta}_2 + m_2 l_2 g c_{12} + (m_1 + m_2)l_1 g c_1$$

$$w_2 = m_2 l_2^2 \ddot{\theta}_1 + m_2 l_1 l_2 c_2 \ddot{\theta}_1 + m_2 l_2 s_2 \dot{\theta}_1^2 + m_2 l_2 g c_{12}$$

Let

$$\dot{\theta}_1 = \omega_1$$

$$\dot{\omega}_1 = \ddot{\theta}_1 = \frac{1}{m_2 l_2^2 + (m_1 + m_2)l_1^2 + I_{m1}}(-w_1 + \tau_1 - B_{m1}\omega_1)$$

$$\dot{\theta}_2 = \omega_2$$

$$\dot{\omega}_2 = \ddot{\theta}_2 = \frac{1}{m_2 l_2^2 + I_{m2}}(-w_2 + \tau_2 - B_{m2}\dot{\omega}_2)$$

putting these above four equations in state-space form, we have

$$\begin{bmatrix} \dot{\theta}_1 \\ \dot{\omega}_1 \\ \dot{\theta}_2 \\ \dot{\omega}_2 \end{bmatrix} = \begin{bmatrix} 0 & 1 & 0 & 0 \\ 0 & \dfrac{-B_{m1}}{m_2 l_2^2 + (m_1 + m_2) l_1^2 + I_{m1}} & 0 & 0 \\ 0 & 0 & 0 & 1 \\ 0 & 0 & 0 & \dfrac{-B_{m2}}{m_2 l_2^2 + I_{m2}} \end{bmatrix} \begin{bmatrix} \theta_1 \\ \omega_1 \\ \theta_2 \\ \omega_2 \end{bmatrix} +$$

$$\begin{bmatrix} 0 & 0 \\ \dfrac{1}{m_2 l_2^2 + (m_1 + m_2) l_1^2 + I_{m1}} & 0 \\ 0 & 0 \\ 0 & \dfrac{1}{m_2 l_2^2 + I_{m2}} \end{bmatrix} \begin{bmatrix} \tau_1 \\ \tau_2 \end{bmatrix} + \begin{bmatrix} 0 & 0 \\ \dfrac{-1}{m_2 l_2^2 + (m_1 + m_2) l_1^2 + I_{m1}} & 0 \\ 0 & 0 \\ 0 & \dfrac{-1}{m_2 l_2^2 + I_{m2}} \end{bmatrix} \begin{bmatrix} w_1 \\ w_2 \end{bmatrix}$$